ISTANBUL TECHNICAL UNIVERSITY ★ GRADUATE SCHOOL

DAMAGE CLASSIFICATION OF CNT/CNC-REINFORCED PU FOAM-CORED SANDWICH PANELS THROUGH ACOUSTIC EMISSION TESTING

M.Sc. THESIS

Eyüphan KÜÇÜKKALFA

Department of Aeronautical and Astronautical Engineering

Aeronautical and Astronautical Engineering Programme

JANUARY 2024

ISTANBUL TECHNICAL UNIVERSITY ★ GRADUATE SCHOOL

DAMAGE CLASSIFICATION OF CNT/CNC-REINFORCED PU FOAM-CORED SANDWICH PANELS THROUGH ACOUSTIC EMISSION TESTING

M.Sc. THESIS

Eyüphan KÜÇÜKKALFA
(511211122)

Department of Aeronautical and Astronautical Engineering

Aeronautical and Astronautical Engineering Programme

Thesis Advisor: Asst. Prof. Kaan YILDIZ

JANUARY 2024

İSTANBUL TEKNİK ÜNİVERSİTESİ ★ LİSANSÜSTÜ EĞİTİM ENSTİTÜSÜ

AKUSTİK EMİSYON YÖNTEMİ İLE KNT/SNK KATKILI PU KÖPÜK DOLGULU SANDVİÇ PLAKALARIN HASAR MEKANİZMALARININ İNCELENMESİ

YÜKSEK LİSANS TEZİ

Eyüphan KÜÇÜKKALFA
(511211122)

Uçak ve Uzay Mühendisliği Anabilim Dalı

Uçak ve Uzay Mühendisliği Programı

Tez Danışmanı: Dr. Öğr. Üyesi Kaan YILDIZ

OCAK 2024

Eyüphan Küçükkalfa, a M.Sc. student of İTU Graduate School student ID 511211122, successfully defended the thesis entitled "DAMAGE CLASSIFICATION OF CNT/CNC-REINFORCED PU FOAM-CORED SANDWICH PANELS THROUGH ACOUSTIC EMISSION TESTING", which he prepared after fulfilling the requirements specified in the associated legislations, before the jury whose signatures are below.

Thesis Advisor : **Asst. Prof. Kaan YILDIZ** ....
Istanbul Technical University

Jury Members : **Asst. Prof. Alptekin YILDIZ** ....
Istanbul Technical University

Asst. Prof. Fatih USTA ....
Gebze Technical University

Date of Submission : 05 January 2024
Date of Defense : 23 January 2024

To my family,

FOREWORD

I would like to extend my appreciation to my esteemed supervisor, Dr. Kaan Yıldız, for giving me a precious opportunity to study under his guidance. I am also grateful of his unwavering support whenever I need his expertise and proficiency.

I am grateful to Dr. Hülya Cebeci for her contributions to my educational life not only for my thesis, but throughout the entire time we worked together. She always supported and encouraged me with her expertise in directing my academic journey.

I am grateful to Dr. Mohammad Fotouhi, Ali Ghaderiaram, and Dr. Sakineh Fotouhi for their tremendous efforts in acoustic emission testing and data analysis. I appreciate them sharing their wealth of information about the acoustic emission method with me and taking the time to carefully address every question I had during our collaboration.

I would like to thank Melisa Dinçer for her efforts in the manufacturing of 3D woven I-beam fabrics, and Çağın Emre and Halil İbrahim Şahin for their assistance in the optimization of the direct foaming procedure within the vacancies of I-beam composites.

This thesis was partially funded by the Scientific and Technological Research Council of Turkey (TUBITAK) 1003 Primary Subjects R&D Funding Program (Project No. 218M703 and Project No. 218M704) and Career Development Program 3501 (Project No. 121M993). I am also grateful to the TUBITAK 2224-A Support Program for Participation in Abroad Scientific Events that supported me in presenting my work at The 20th European Conference on Composite Materials (ECCM20).

Lastly, I express my infinite gratitude to my beloved family, whose impacts on my entire educational journey are at least as significant as mine, not just during my thesis process. I am thankful to my mother, Zeynep Küçükkalfa, who instilled in me a love for reading through the countless pages of books she read at night. I am also grateful to my father, Adnan Küçükkalfa, who attempted to assist me with brainstorming sessions for every technical problem I encountered.

January 2024

Eyüphan KÜÇÜKKALFA
(Aeronautical Engineer)

TABLE OF CONTENTS

Page

ABBREVIATIONS

2D	: Two Dimensional
3D	: Three Dimensional
AE	: Acoustic Emission
ASTM	: American Standard Test Method
CNC	: Cellulose Nanocrystal
CNF	: Carbon Nanofiber
CNT	: Carbon Nanotube
DCB	: Double Cantilever Beam
KNT	: Karbon Nanotüp
LBX	: Load Bearing X Vertical Wall
UTM	: Universal Testing Machine
PU	: Polyurethane
PVC	: Polyvinylchloride
PMDI	: Polymeric Diphenylmethane Diisocyanate
PMI	: Polymethacrylimide
Rpm	: Revolutions per minute
SNK	: Selüloz Nanokristal
SEM	: Scanning Electron Microscopy
VARTM	: Vacuum-assisted Resin Transfer Molding Method
WT	: Wavelet Transform
Wt.%	: Weight Percentage

SYMBOLS

°C	: Celsius Degree
A	: Cross section area
dB	: Decibel
ϵ_c	: Compressive strain
ϵ_f	: Flexural strain
h	: Stroke
h_0	: Initial height
kHz	: KiloHertz
kg	: Kilogram
kN	: KiloNewton
l	: Cell edge length
m^3	: Cubic meter
MPa	: MegaPascal
σ_c	: Compressive stress
σ_f	: Flexural stress
t	: Cell wall thickness

LIST OF TABLES

Page

LIST OF FIGURES

Page

DAMAGE CLASSIFICATION OF CNT/CNC-REINFORCED PU FOAM-CORED SANDWICH PANELS THROUGH ACOUSTIC EMISSION TESTING

SUMMARY

Aerospace companies are making significant attempts to design highly-efficient lightweight aircraft while satisfying the required mechanical properties and allowing increased volume for the payload. Composite structures, specifically sandwich composites, have widespread use in the aviation industry owing to their high strength-to-weight ratio when compared to standard metal-aluminum construction materials. Although honeycomb sandwich composites have high impact resistance, they have disadvantages such as moisture absorption, water accumulation, and debonding due to the open-cell structure of the honeycombs. Accordingly, rigid polymeric foams with a closed-cell core structure are capable of overcoming these disadvantages and replacing honeycombs in future applications.

Closed-cell and rigid polyurethane (PU) foams are valuable since they have an easy manufacturing process, multifunctionality, and capacity for reinforcement studies. Carbon nanotubes (CNTs) frequently serve as reinforcement materials in PU foams owing to their superior strength and light weight. However, when the concentration of CNT reinforcement is relatively high, disadvantages such as agglomeration and nonuniform dispersion may occur in the foam structure, leading to poor mechanical properties of the materials. Therefore, reinforcing CNTs into PU foams by hybridizing them with auxiliary materials such as cellulose nanocrystals (CNCs) might be an efficient alternative approach to the dispersion problem. The hybridization with CNCs can prevent the formation of strong Van der Waals bonds between CNTs.

Ensuring passenger safety in aircraft requires prompt detection of any potential damage. Despite several benefits of foam-filled sandwich composites, they also have particular damage mechanisms that may occur under high loadings. The non-destructive testing method called *acoustic emission (AE) testing* allows real-time identification of transient elastic waves that are released from the defect source by sensors and classification of these failure mechanisms. Unlike other non-destructive testing techniques such as electromagnetic, radiographic, and ultrasonic, AE analyzes the failure tendency and prevents potentially irreversible damage by using data released directly from the defect source. Nevertheless, it is necessary to use a clustering method to categorize AE data into appropriate clusters that are each associated with a possible damage mechanism. Among manual clustering, signal processing, supervised clustering and unsupervised clustering; unsupervised clustering arises due to their great performance in first-time analysis of AE hits without having a historic data of the experiment. The performance of the k-means algorithm, which is one of the most efficient unsupervised clustering methods, heavily depends on the first cluster centers, and it often gets stuck at local minima. Hence, the k-means genetic

algorithm can resolve this challenge through improved searching capacity that can provide an optimum solution in a reasonable amount of time.

Previous research in the literature mainly studied the AE analysis of sandwich composites with honeycomb and foam cores, but there is a lack of research on sandwich composites with nanomaterial reinforcement of core materials. The thesis investigated the impact of reinforcement studies on the damage mechanisms of CNT/CNC-reinforced foam-cored sandwich composites through the AE test system. Damage mechanisms were classified using peak frequency, amplitude, and cumulative energy of AE data by the k-means genetic algorithm. In addition, as a subsection, the bending properties of CNT-reinforced PU foam-filled 3D woven I-beam composites were studied. Thus, a preliminary study was performed for CNT reinforcement studies on PU foam and its combination with sandwich composites. Furthermore, this preliminary study was beneficial for understanding the influence of PU foams on sustaining structural integrity and avoiding damage mechanisms in composite structures.

AKUSTİK EMİSYON YÖNTEMİ İLE KNT/SNK KATKILI PU KÖPÜK DOLGULU SANDVİÇ PLAKALARIN HASAR MEKANİZMALARININ İNCELENMESİ

ÖZET

Yüksek verimli uçakların tasarlanırken gerekli mekanik özelliklerin karşılanması ve faydalı yük için daha fazla alan oluşturulması havacılık ve uzay şirketlerinin en önemli tasarım koşullarındandır. Kompozit yapılar, özellikle sandviç kompozitler, standart metal-alüminyum yapı malzemelerine göre yüksek mukavemet/ağırlık oranına sahip olmaları nedeniyle havacılık endüstrisinde yaygın kullanıma sahiptir. Sandviç kompozitler genelde yüzey katmanı (face sheet), çekirdek (core) ve opsiyonel olarak yüzey katmanı ile çekirdek malzemesi arasında bulunan yapışkan filmden oluşur. Çekirdek malzemesi olarak ise balpeteği yapılar veya polimerik köpük dolgusunun kullanılması oldukça yaygındır. Balpeteği yapılı sahip sandviç kompozitlerin darbe dayanımı yüksek olmasına rağmen, balpeteği yapıların açık hücre geometrisinden dolayı nem emme, su biriktirme ve yapışma ayrılması (debonding) gibi dezavantajları bulunmaktadır. Bundan dolayı, kapalı hücreli çekirdek yapısına sahip sert polimerik köpükler, bu dezavantajların üstesinden gelme ve gelecekteki uygulamalar için balpeteklerinin yerini alma kapasitesine sahiptir. Polimerik köpükler kapalı hücre yapısı sayesinde yüzey katmanı ile daha etkin yapışma sağlarlar ve böylece hücre aralarına su girmesi engellenir.

Kapalı hücreli ve sert poliüretan (PU) köpükler, kolay imalat sürecine sahip olmaları, multifonksiyonel olmaları ve katkılama çalışmalarına elverişli olmaları nedenleriyle sandviç köpüklerin dolgu malzemesi olarak öne çıkmaktadır. PU köpüklere yapılabilen nanokatkılama çalışmaları sonucunda yapının mekanik, termal, akustik gibi malzeme özelliklerinde iyileştirmeye yönelik çalışmalar yapılabilir. Karbon nanotüpler (KNT) ise üstün mukavemet özellikleri ve hafif olmaları nedeniyle PU köpüklerin nanomalzeme katkılama çalışmalarında sıklıkla kullanılmaktadır. Bununla birlikte, katkılama çalışmalarındaki KNT konsantrasyonun nispeten yüksek olduğu durumlarda ise köpük içerisinde topaklanma ve homojen olmayan dağılım gibi dezavantajlar meydana gelmektedir. Bu da PU köpüğün malzeme değerlerinde düşüşe yol açabilir. Bu nedenle, yüksek konsantrasyonlardaki KNTlerin katkılama çalışmalarında bu sorunu ortadan kaldırmak için farklı stratejiler denenmektedir. Bu doğrultuda, bu çalışmada, KNTlerin kendileri ile kimyasal olarak uyumlu bir malzeme olan selüloz nanokristal (SNK) ile birlikte hibridize edildikten sonra PU köpüğe katkılama yapılırsa dispersiyon problemine etkili bir çözüm olacağı öngörülmüştür. Çünkü SNKler ile KNTler suda disperse edilirse, SNKlerin hidrofilik kısımları su ile bağ yaparken hidrofobik kısımlarının ise KNTler ile bağ yapacağı düşünülmektedir. Böylece, KNTlerin kendi arasındaki güçlü Van der Walls bağlarının etkisinin azaltılacağı öngörülmektedir. Böylece, KNTlerin daha yüksek oranlarda nanomalzeme katkılaması yapılarak optimum değerin bulunmasına yönelik çalışmalar yapılabilecektir.

Güvenli uçuş koşullarının sağlanabilmesi için uçuş öncesindeki ve uçuş esnasındaki yapılan kontrollerde olası arızaların hızlı bir şekilde tespit edilmesi oldukça önemlidir. Bu sebeple hava-uzay araçlarında kullanılan malzemelerin olası hasar mekanizmalarının belirlenmesi ve bu hasar mekanizmaları geciktirilerek veya ortadan kaldırılarak güvenli uçuş koşullarının sağlanabilmesi gerekmektedir. Köpük dolgulu sandviç kompozitlerin birçok avantajının yanı sıra, artan yükler altında oluşabilecek bazı hasar mekanizmaları da vardır. *Akustik emisyon (AE) testi* olarak adlandırılan tahribatsız muayene yöntemi, malzeme yüzeyine entegre edilen sensörler tarafından hasar kaynağından yayılan geçici elastik dalgaların gerçek zamanlı olarak yakalanmasına ve bu hasar mekanizmalarının sınıflandırılmasına olanak sağlar. Elektromanyetik, radyografik ve ultrasonik gibi diğer tahribatsız muayene tekniklerinden farklı olarak AE, hasar eğilimini analiz eder ve doğrudan hasar kaynağından yayılan verileri kullanarak geri dönüşü olmayan potansiyel hasarların önlenmesine yardımcı olan bir yapısal sağlık izleme yöntemidir.

Ancak, hasar kaynağından toplanan AE verilerinin özellikle hangi hasar mekanizmasına ait olduklarının tespit edilebilmesi için uygun bir kümeleme yöntemi kullanılarak AE verilerini sınıflandırılması gerekmektedir. Bu sınıflandırmada ise AE verilerinin genlik, kümülatif enerji, frekans aralığı, yükselme süresi, eşiği geçen AE veri sayısı, gibi özellikleri kullanılmaktadır. Manuel kümeleme, sinyal işleme, denetimli kümeleme ve denetimsiz kümeleme arasında; denetimsiz kümeleme, deneyin geçmiş verilerine sahip olmadan AE datalarının ilk kez analizindeki üstün performanslarından dolayı öne çıkmaktadır. Çünkü denetimli kümeleme yöntemi her ne kadar daha gelişmiş bir yöntem gibi gözükse de literatürdeki geçmiş verilerin kullanılması elde edilen dataların yanlış yorumlanmasına yol açabilmektedir. Çünkü, test edilen ortam, kullanılan malzeme, sensör konumları, data ayıklama sistemi, ve testi yapan kişinin uzmanlığı gibi parametreler deneyden deneye oldukça farklılık gösterebilmektedir.

En etkili denetimsiz kümeleme yöntemlerinden biri olan k-means algoritmasının performansı büyük ölçüde ilk küme merkezlerine bağlıdır ve sıklıkla yerel minimumlara takılıp kalır. Dolayısıyla k-ortalamalar genetik algoritması, makul bir sürede optimum çözümü sağlayabilmesi ve her iterasyonda kümeleri güncellemesi gibi gelişmiş arama kapasitesi sayesinde AE verilerini kümelere ayırmada daha etkin bir çözüm ortaya koymaktadır. Böylece, geçmiş deney verilerinin olmadığı ilk defa yapılan çalışmalarda en uygun kümeleme işlemi gerçekleştirilene kadar genetik algoritma tekrar eder ve AE verilerinin sınıflandırılması en uygun şekilde yapılmış olur.

Literatürdeki makaleler incelendiğinde balpeteği yapılı ve köpük dolgulu sandviç kompozitlerin AE analizi üzerine çeşitli çalışmaların yapıldığı gözlemlenmiştir. Ancak köpük dolgulu sandviç kompozitlerdeki köpük dolgusunun nanomalzeme ile katkılanmasının hasar mekanizmalarına olan etkisinin incelenmesine yönelik pek fazla çalışmaya rastlanmamıştır. Bu tez kapsamında, PU köpüğün hibrit KNT/SNK malzeme ile katkılandırılmasının köpük dolgulu sandviç kompozitlerin hasar mekanizmaları üzerindeki etkisi AE test sistemi aracılığıyla incelenmiştir. Hasar mekanizmaları, k-ortalamalar genetik algoritması ile AE verilerinin tepe frekansı, genliği ve kümülatif enerjisi kullanılarak sınıflandırılmıştır. Ayrıca bir alt bölüm olarak karbon nanotüp ile güçlendirilmiş PU köpük dolgulu üç boyutlu dokuma I kiriş kompozitlerinin eğilme özellikleri incelenmiştir. Böylece sandviç kompozit yapılarla çalışmaya başlamadan önce, KNT katkılamasının PU köpüğün basma özelliklerine ve köpük dolgulu I kirişin eğilme davranışına olan etkisi test edilmiştir. Ayrıca bu ön çalışma, PU köpüklerin üç boyutlu dokuma I kiriş kompozitlerin yapısal bütünlüğüne ve hasar mekanizmalarının ortadan kaldırılmasına olan etkisinin anlaşılması için faydalı olmuştur.

1. INTRODUCTION

In the aviation industry, companies are making great efforts to design highly-efficient lightweight aircraft while satisfying the desired mechanical properties and freeing up increased volume for the payload and useful load. Payload means the weight of the passengers, luggage, and cargo for which the aircraft generates income, and useful load indicates the weight of the flight crew, fuel, and drainable oil for airliners [1]. Especially for civil aviation, where a small percentage of annual profit is enough to sustain flight operations, each kilogram as a payload has a crucial effect on the company's balance of income and expenses [2]. Therefore, composite structures have a widespread field of application in the aviation industry due to their high strength-to-weight ratio compared to conventional metal-aluminum construction materials [3]. Laminated composites can provide 40% and 20% weight savings for secondary structures (doors, fairings, elevator, rudder, etc.) and primary structures (wings, fuselage, etc.), respectively [4]. For example, Piquet states that 53% of the primary load-bearing structures of the Airbus A350 XWB were manufactured from carbon fiber-reinforced composites to make the fuselage lighter [5].

Sandwich composites are structural materials that stand out with their low weight compared to laminated composites of the same size. While sandwich composites constitute 8% of the Boeing 707’s wet surface, this amount rises to 46% for Boeing 757 and 767 [6]. Moreover, sandwich composites are important not only for their low densities but also for improved bending properties. As two main components of sandwich composites, face sheets are exposed to greater stresses under bending load, whereas the core distributes and weakens the stress wave among two face sheets [7]. The face sheets in sandwich panels stand the majority of the tensile and compressive loads that arise from bending, and the core bears the majority of the shear stress perpendicular to the surface [8].

Sandwich composites are categorized based on their core material, which is typically foam or honeycomb. Nose landing gear doors, spoilers/ailerons, cabin floor panels, fuselage belly fairing, pylons/nacelles, vertical tail plane, several wing components such as leading-edge panels and access panels, and flap tracking fairings of Airbus A380 are made of different types of sandwich composites as shown in Figure 1.1 [9]. Despite their high impact resistance, honeycomb sandwich composites have disadvantages such as moisture absorption, water accumulation, and debonding due to the open-cell structure of the honeycombs [7]. Therefore, rigid foams with a closed-cell structure have the potential to overcome these disadvantages and replace honeycombs in future applications.

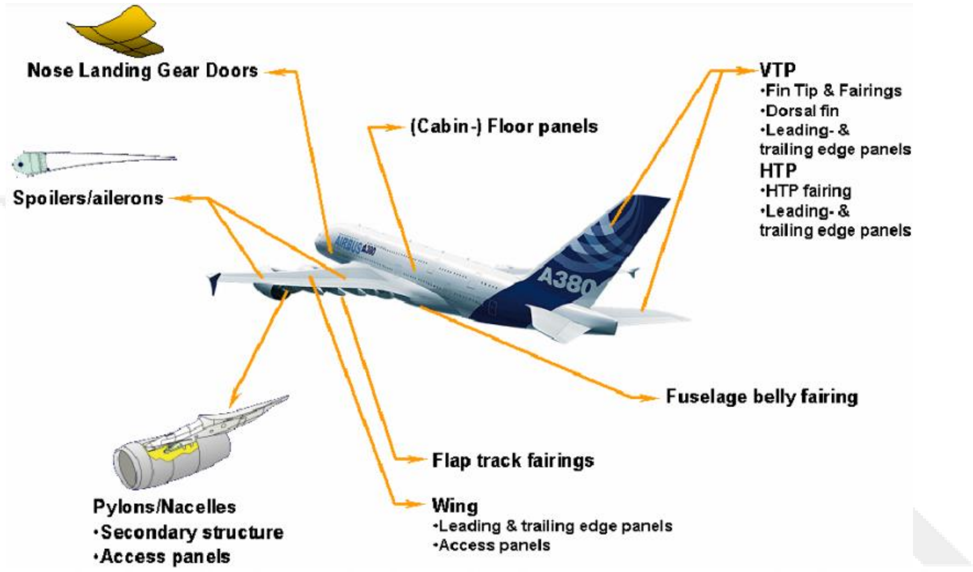

Figure 1.1 : Sandwich composite usage in Airbus A380 [9].

1.1 Multifunctional PU Foams

In recent years, polyurethane (PU), polyvinylchloride (PVC), and polymethacrylimide (PMI) foam materials have been frequently used in the manufacturing of sandwich composites [10]. Among these, closed-cell and rigid PU foams are salient because of their ease of process and multifunctionality [11]. PU foams of different densities can be used as structural support and safeguarding elements in aviation and space applications. Moreover, researchers have been working on improving the mechanical properties of PU foams and adding multifunctionality through nanomaterial reinforcement. Polymeric foams can be strengthened by material reinforcement, including carbon nanotubes (CNTs) [12, 13], carbon nanofibers (CNFs) [14], nanoclays [15], titanium dioxide [15], aluminum oxide [16], cellulose nanocrystals (CNCs) [17], and glass fibers [18-20]. Ciecierska et al. [12] enhanced the strength of PU foams using CNTs up to 0.05 wt.%. The study demonstrated a 21% improvement in bending strength. Furthermore, Navidfar et al. [13] enhanced the strength of PU foams by 0.25 wt.% CNT reinforcement, resulting in a significant 15% improvement in tensile strength. In addition, Zainuddin et al. [14] employed CNF as a reinforcement in PU foam-cored sandwich composites and effectively obtained a 19% increase in shear modulus and a 33% increase in shear strength. The study conducted by Saha et al. [15] investigated the effects of combining titanium dioxide and nanoclay into PU foams. The results showed that nanoclay improved the tensile modulus by 69.3%, while TiO_2 increased the compressive modulus by 12.4%. Furthermore, Septevani et al. achieved a 16.74% improvement in compressive modulus by CNC reinforcement [17]. Moreover, Şerban et al. and Yu et al. achieved increases of 68.9% and 35% in the tensile modulus [18] and compressive strength [19], respectively, by reinforcing PU foams with glass fibers.

1.1.1 CNT/CNC interaction

Owing to their outstanding strength and light weight, carbon-based materials such as CNTs and CNFs frequently serve as reinforcing agents. Nevertheless, when the quantity of CNT reinforcement is relatively high, drawbacks such as agglomeration and nonuniform dispersion arise in the foam structure, resulting in poor mechanical properties of the materials [21]. Therefore, researchers frequently investigate the development of various strategies to achieve the efficient dispersion of nanomaterials within the polymers. Kabir et al. conducted a study on enhancing the mechanical properties of PU foams through ultrasonic dispersion of CNFs [22]. The study revealed that CNFs were unable to achieve efficient dispersion due to the increased viscosity, which posed challenges in the process conditions. In order to solve this situation, separate dispersion studies were conducted on the raw materials, isocyanate and polyol components, of the proposed PU foams. With this approach, a 10% increase in compressive strength was achieved by 0.5% CNF reinforcement of PU foams. Moreover, enhanced mechanical properties have been achieved in complex and difficult-to-disperse structures such as CNTs through the inclusion of functional groups via mechanical techniques and/or highly acidic processes [7]. Çağlayan et al. incorporated mechanical mixing optimization into the PU reinforcement experiments involving CNTs, both with and without the carboxly (COOH) functional group [7]. This resulted in an enhancement of compressive strength, with a maximum 13.4% increase observed by 0.1% CNT reinforcement. These studies consistently found that enhancing the interactions between polymers and CNTs and ensuring their effective distribution were crucial factors in improving the mechanical performance of PU foams.

Xu et al. stated that adding CNTs into PU foams by hybridizing with external materials such as CNCs and CNFs might be an effective alternative solution for dispersion problems [23]. For instance, the insertion of additional nanomaterials such as CNCs can impede the formation of strong Van der Waals bonds between CNTs [24]. This promotes the uniform distribution of the foam structure. Distilled water is considered to be one of the most readily available and suitable liquids for efficiently dispersing CNTs and CNCs. As a result of the chemical composition of CNCs, they exhibit colloidal stability by forming bonds with CNTs through non-polar regions shown in Figure 1.2a and with distilled water through hydrophilic regions illustrated in Figure 1.2b [25, 26]. After evaporating distilled water to vaporization, it is possible to enhance the strength of polymeric foams by reinforcing with the most effective concentration of CNT/CNC powder.

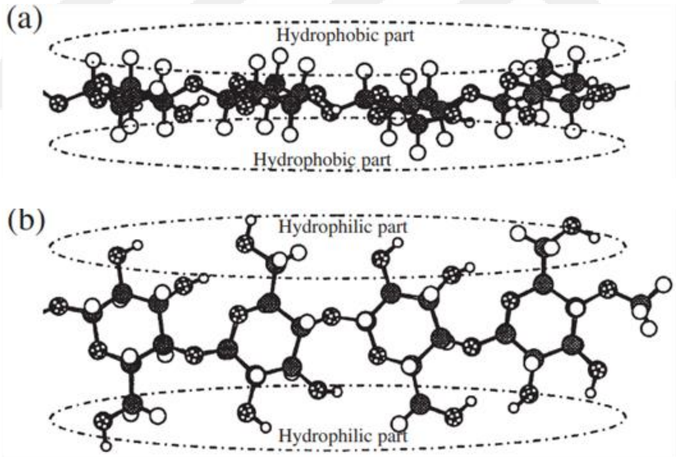

Figure 1.2 : A ring plane of cellulose molecule from a) end view and b) front view [26].

1.1.2 PU foams for the structural support of beams

Polymeric foams not only serve as a core material in sandwich composites but also enhance the structural integrity of beam structures. Akrami et al. [27] designed bio-inspired T-joint structures inserting PVC foams into the intersection point of the web and flanges as shown in Figure 1.3. T-joint showed superior mechanical performance with a 40% increase in peak load during bending and a 60% increase in stiffness. Moreover, this concept can readily be applied to I-beams. Alternatively, rather than positioning the polymeric foam at the intersection of the web and flanges, filling this space with PU foams could potentially result in even greater improvements in strength and stiffness and preserve structural integrity. For instance, Lacki and Derlatka [28] inserted PU foams into the area between the web and flanges of an aluminum alloy I-beams made of two combined C beams. This resulted in a 200% enhancement in the beam's buckling resistance. Nevertheless, the presence of stress concentration points and the complexity of the design processes emerged as a result of the lap joints utilized to form an I-beam profile using two C-beam profiles. Moreover, Safari et al. [29] conducted a study where they inserted PU foams into the area of 3D woven pile yarn composites, resulting in a 270% increase in the core shear modulus.

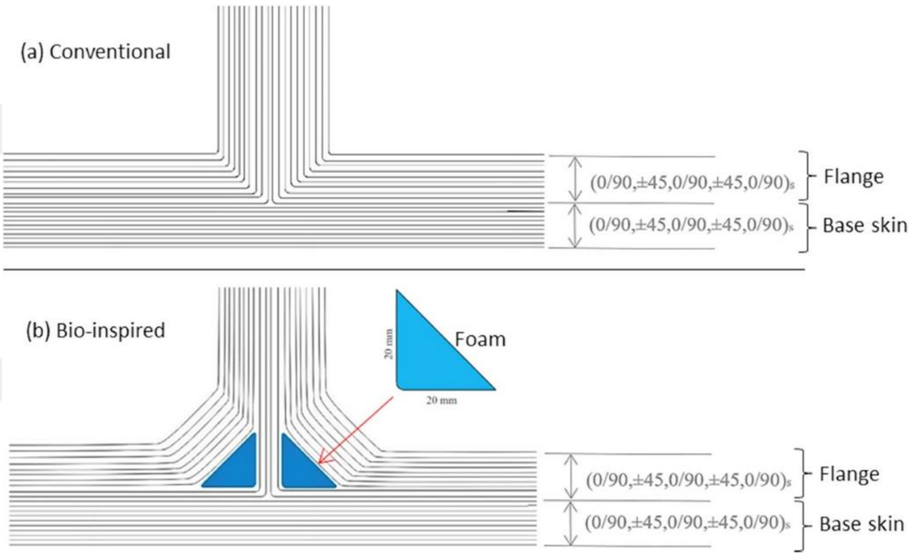

Figure 1.3 : T-joints with PVC foam: (a) Conventional and b) bio-inspired. [27].

1.1.3 PU foam-integrated 3D woven I-beam composites

Beam profiles can experience several failure mechanisms such as web yielding, web buckling, and flange crushing. Several studies have attempted to address the web section by inserting core materials into the gaps between the flanges and the web [30,31]. Because the web section is unable to withstand shear loads under high loading, failure on near mid-span and web buckling near support is inevitable as shown in Figure 1.4 [31]. These materials have demonstrated the capacity of enhancing bending properties and structural integrity by retarding web yielding and buckling. Moreover, 3-D woven structures have been under investigation because they have the potential to prevent delamination and enable the design of complex geometries [32,33]. Manufacturers can easily apply 3-D weaving techniques to develop delamination-free structural composites, such as I-beam structures. Therefore, jointless- and delamination-free high-performance I-beam composites can be manufactured.

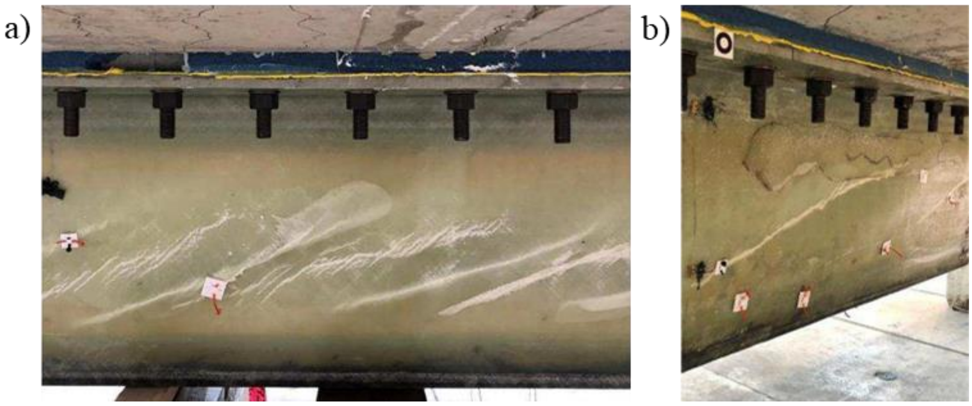

Figure 1.4 : Post-failure images of fiber-reinforced polymer girder including a) failure on near mid-span and b) web buckling near support [31].

The majority of reinforcement studies of polymeric foams in structures having vacancies do not specifically address the process of in-situ foaming within the vacancies. Nevertheless, it is indisputable that manually placing appropriately sized polymeric foams to fill vacancies in structures does not significantly enhance the adhesion between the foam and the composites [34]. Conducting the foaming process directly within the vacancies enhances the bonding between materials, thereby undeniably improving the structural integrity and mechanical responses [35]. Therefore, instead of cutting PU foams into desired dimensions and inserting them into the vacancies of I-beam composites, directly foaming within these vacancies is a great alternative to achieve better adhesion and structural integrity between foam and I-beam structures.

1.2 Acoustic Emission Testing

The detection of any potential damage in aircraft is critical for ensuring the safety of passengers. Although foam-filled sandwich composites have several benefits, they also have certain damage mechanisms that may occur under increased load. For example, Kucukkalfa et al. observed that the PU foam integrated I-beam composites have damage mechanisms such as flange-core debonding, web-core debonding, adhesive bond failure, core crack, matrix cracking, and fiber breakage under compression and three-point bending tests via fractography analysis as shown in Figure 1.5 [36]. According to Assarar et al., foam-filled sandwich composites commonly experience core damage, matrix cracking, fiber matrix separation, interface rupture, and fiber breakage as different types of damage mechanisms [37]. The non-destructive testing method called *acoustic emission (AE) testing* enables real-time detection of transient elastic waves emitted from the defect source by sensors and classification of these failure mechanisms through a data acquisition system [38,39].

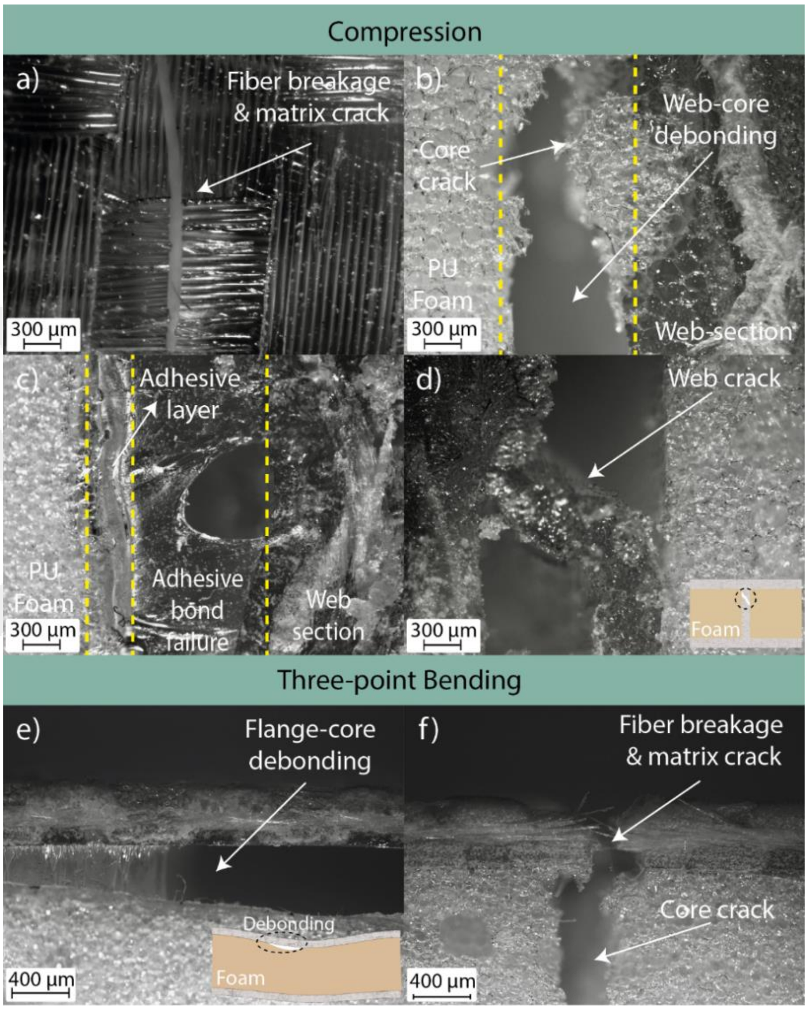

Figure 1.5 : Damage mechanisms of PU foam-filled I-beam composites under compression and three-point bending tests [36].

AE systems are appropriate for conducting research and development studies in laboratories, as well as for quality inspection on production lines. Additionally, they are effective in real-time detection of cracks and leaks in aircraft, spacecraft, and storage tanks [40]. Unlike other non-destructive testing techniques such as electromagnetic, radiographic, and ultrasonic, AE uses data released directly from the defect source to analyze the failure tendency and prevent any potentially irreversible damage.

The instruments used in the AE test system are important in terms of the sensitivity and accuracy of the analysis. Generally, piezoelectric sensors are utilized to capture elastic waves propagating from the defect because they are sensitive and less responsive to mechanical noise [40]. Following the conversion of mechanical waves into electrical signals, the generated signals are amplified by a preamplifier to minimize electromagnetic interference as shown in the schematic representation of AE testing instrumentation in Figure 1.6 [41]. Moreover, since AE studies are carried out at ultrasonic frequencies, high-gain amplifiers (40 dB = 100 times) are needed due to the small amplitude of ultrasonic signals. The bandwidth generally chosen for the most common sensors is 100–300 kHz [40]. These obtained data are digitized and fed to the AE computer for data storage, analysis, and display [41]. In other words, electrical signals are converted into electronic data sets. Simultaneously, parametric data signals (load, strain, temperature, etc.) are also transferred to the system to be used in the analysis.

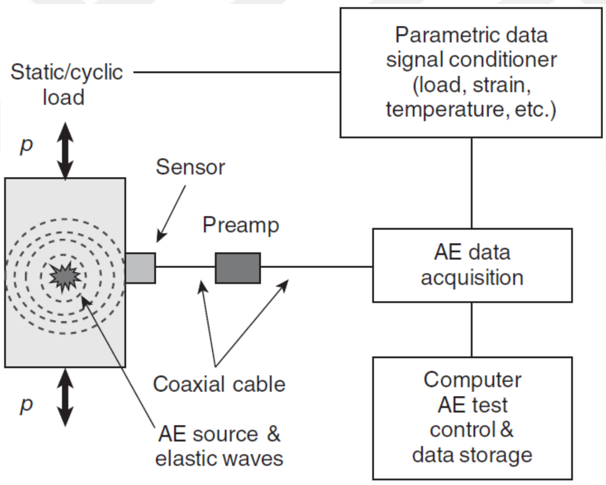

Figure 1.6 : Schematic representation of AE testing instrumentation [41].

AE is defined as events in which one or more local sources subjected to stress emit energy and generate temporary elastic waves which are called Lamb waves as well [40]. Moreover, materials that surpass the critical stress values undergo the occurrence of local (micro-scale) defects, leading to the sudden release of stored strain energy and the initiation of mechanical stress waves [42]. AE signals are captured by sensors to detect and analyze Lamb waves that are generated from defects. These signals are utilized to classify damage mechanisms based on specific AE characteristics, including rise time, amplitude, decay time, and the number of waves that exceed the threshold required for detection as illustrated in Figure 1.7 [41]. In some studies, researchers utilized the first AE event for laminated composites [43,44], the first high-energy AE events [45,46], and wave numbers passing the first threshold to detect and trace one type of damage mechanism. Additionally, researchers utilized cumulative curves to examine multiple damage mechanisms, including the first AE events [47,48], energy [49,50], and wave numbers crossing the threshold [51,52].

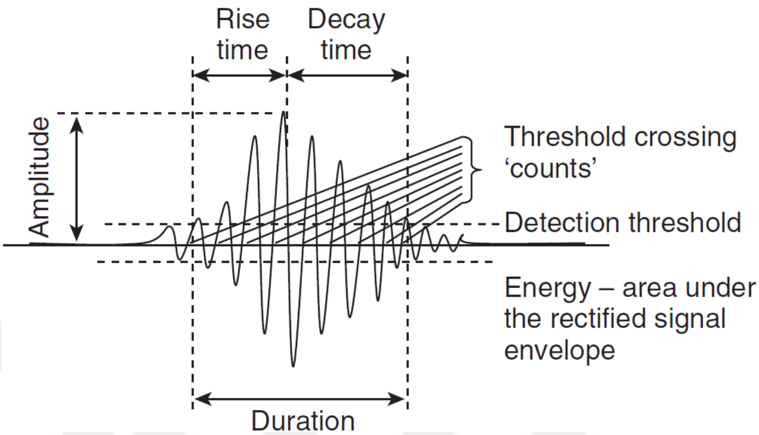

Figure 1.7 : AE characteristics to classify damage mechanisms [41].

1.2.1 Clustering Algorithms

Several studies utilize AE for structural health monitoring and damage detection in composites. Bohse concluded that AE tests during double cantilever beam (DCB) tests can group damage mechanisms for laminated composites by estimating amounts and controlling the power spectra of AE waves [53]. Moreover, Haselbach and Lauke used power spectra to detect damage in glass fiber composites under tensile load [54]. However, it is necessary to apply a clustering method to separate AE data into proper clusters each of which belongs to a potential damage mechanism. Researchers can use four clustering technique types — manual clustering, unsupervised clustering, supervised clustering, and signal processing — to classify AE data into distinct damage mechanisms. Some studies [55-57] manually classified AE data based on one or two parameters, such as peak frequency and amplitude, and associated them with different damage types. However, the manual classification of AE parameters may not always convincingly separate damage mechanisms without additional correlation strategies. Therefore, researchers often implement machine learning techniques to account for the complex relationship between AE parameters in both unsupervised and supervised clustering. The damage modes in composite materials can be distinguished by unsupervised clustering techniques such as k-means, fuzzy c-means, Gaussian mixture distribution, self-organizing map, and hierarchical models [58]. The k-means algorithm is more common and successful in detecting damage mechanisms of composite structures [59,60]. In addition, k-means++ is an unsupervised learning algorithm that optimizes the distance between vectors within a cluster. Until the significant changes in clustering data points are overcome, the algorithm selects a single point at random from the AE dataset [61]. On the other hand, supervised clustering algorithms are developed with learned data and then applied to unknown datasets. While supervised clustering may yield closer results under repeated test conditions, unsupervised clustering methods are crucial for the first-time analysis. Researchers also use signal processing methods, such as wavelet transform (WT), to classify damage types. The WT method divides a signal into low- and high-frequency sub-parts [62], enabling the association of these sub-parts with specific damage types based on their frequencies.

1.2.1.1 K-means genetic algorithm

In the first step of the k-means algorithm, AE data can be clustered by randomly selecting centroids, and in the second step, cluster centers are updated. Nevertheless, the k-means algorithm's performance is highly dependent on the first cluster centers, and it is prone to becoming stuck at local minima [63]. Therefore, genetic algorithms can solve this problem through enhanced searching capacity that can deliver an ideal solution in a reasonable amount of time [64,65]. The flowchart in Figure 1.8 summarizes the data clustering mechanism in the k-means genetic algorithm [63]. In the first step, the centers of clusters are selected randomly from the input data set to initialize the population. Secondly, each data point is allocated to the closest cluster center, and then new centers are created using equation 1.1.

$$z_i^* = \frac{1}{n_i} \sum_{x_j \in C_i} x_j \, , i = 1,2, \ldots, k \qquad (1.1)$$

where z_i^* is the new cluster center, x_j is each data point and n_i is the number of points belonging to cluster C_i.

Then, the fitness function is calculated by taking the average of the Euclidean distances between the points and their respective cluster centers as given in equation 1.2. The minimum fitness value is essential for optimal clustering. Then, for this work, Roulette wheel selection [66] with elitist selection was used to select two parents from a population and create two new children based on their fitness values. Elitist selection ensures that the best solution discovered thus far is preserved without any alterations in a new population, ensuring its survival until the end [63]. After the selection, two parents transfer their data to generate new children with a defined crossover probability. Afterwards, the mutation occurs using equation 1.3. Eventually, the algorithm must be iterated until the stopping criterion is triggered. The stopping criterion in this work was defined as the maximum number of iterations.

$$\text{Fitness value} = \sum_{i=1}^{k} \sum_{x_j \in C_i} \left\| x_j - z_i \right\| \tag{1.2}$$

where z_i denotes cluster center, and k is the number of clusters.

$$r' = \begin{cases} r \ x\ (1 \pm 2\Delta) & \text{if } r \neq 0 \\ (\pm 2\Delta) & \text{if } r = 0 \end{cases} \tag{1.3}$$

where r and r′ are gene position values before and after mutation, respectively, Δ is a uniformly distributed number in the range between 0 and 1.

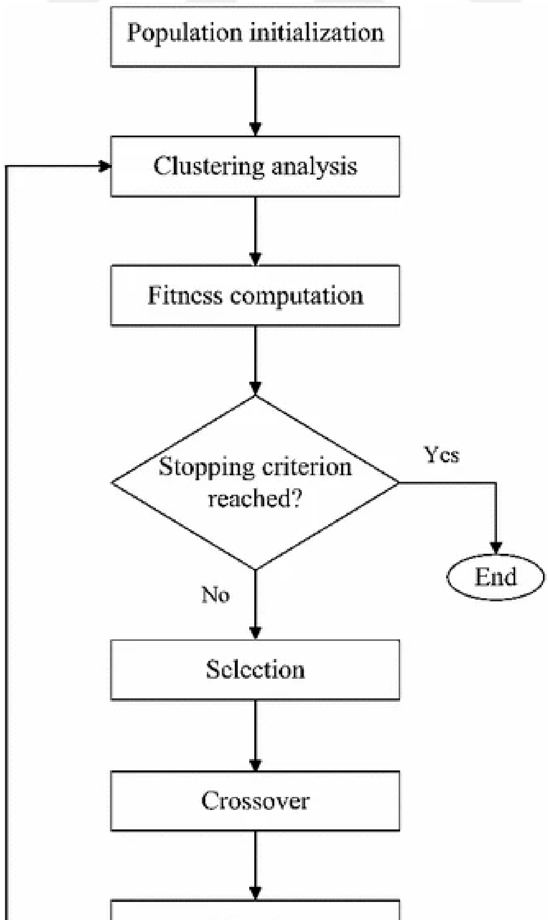

Figure 1.8 : Flowchart of k-means genetic algorithm [63].

1.2.2 Damage classification in sandwich composites

There are various studies in the literature on classifying the damage mechanisms of materials using AE testing. Table 1.1 compiles the studies that utilize the AE system to detect damage mechanisms in sandwich composite materials. Quispitupa et al. investigated the damage mechanisms of honeycomb-cored sandwich composites under tensile tests simultaneously with AE tests [67]. However, since any clustering method is not applied to AE data, the amplitude and energy of AE data are divided by certain limits for each damage mechanism. Thus, it was not possible to effectively separate AE data belonging to different damage mechanisms at similar energy levels and frequencies. Similarly, in the studies that analyzed solely amplitude data, it was not sufficient to cluster AE data effectively, even though they used clustering algorithms [37,39,68]. Therefore, to overcome this uncertainty, several authors recommended the use of peak frequency, cumulative energy data, and amplitude for well-distinguished damage classification [63,69]. For example, Pashmforoush et al. [63] applied the k-means genetic algorithm to the peak frequency and the cumulative energy AE data of PET-cored sandwich composites under the DCB test and classified damage mechanisms as core damage, adhesive failure, matrix cracking, and fiber breakage. Moreover, AE data of sandwich composites with auxetic cores subjected to an indentation test and PEI cores under a three-point bending test, respectively [70,71], were classified by using amplitude ranges of damage mechanisms determined by previous studies in the literature. However, using reference AE data for different composite materials under different tests may lead to a misinterpretation of the results. Furthermore, some studies [61,72] utilized amplitude and peak frequency data, which gave reliable results in the clustering of damage mechanisms. Osa-uwagboe et al. investigated the damaged mechanisms of PVC-cored sandwich composites under the indentation test by clustering AE data with the k++ means algorithm, which is an alternative way to the random initialization used by k-means [61]. Besides the amplitude and peak frequency of AE data, cumulative energy gives an opinion about how each damage mechanism affects the failure of the specimens [73,74].

Table 1.1 : A summary of AE test applications for damage detection in sandwich composites.

Face Sheet /Core	Test	Clustering Algorithm	Damage Mechanisms	AE Characteristics			Ref
				Amplitude (dB)	Energy (aJ)	Frequency (kHz)	
Carbon Fiber/ Honeycomb	Tensile	-	Core Damage	45-60	0-25	-	[67]
			İnterface Failure	60-80	3-219	-	
			Matrix Cracking	80-90	88-374	-	
			Fiber Breakage	Above 90	347-13568	-	
Glass Fiber/PVC Foam	3PT Bending	Fuzzy C-means	Matrix Cracking	40-65	-	-	[37]
			Debonding	40-75	-	-	
			İnterface Failure	50-90	-	-	
			Delamination	50-85	-	-	
			Fiber Breakage	80-100	-	-	
Glass Fiber/PVC Foam	4PT Bending	Fuzzy C-means	Core Damage	36-60	-	-	[68]
			Matrix Cracking	68-80	-	-	
			Fiber Breakage	Above 90	-	-	
			Debonding	80-89	-	-	
Glass Fiber/PVC Foam	3PT Bending	K-means	Core Damage	40-58	-	-	[39]
			Debonding	72-100	-	-	
			Matrix Cracking	40-76	-	-	
			Fiber Breakage	Above 94	-	-	
Glass Fiber/PET Foam	DCB	K-means genetic	Core Damage	40-60	0-30	30-80	[63]
			Adhesive Failure	60-80	5-230	100-150	
			Matrix Cracking	75-85	90-390	160-250	
			Fiber Breakage	85-105	350-1250	250-500	
Glass Fiber/PET Foam	DCB	WT	Core Damage	40-60	0-30	30-65	[69]
			Adhesive Failure	60-80	5-230	100-130	
			Matrix Cracking	75-85	90-390	170-250	
			Fiber Breakage	85-105	350-1250	350-450	
PLA/PLA	Indentation Test	K-means	Core Damage	40-55	-	-	[70]
			Matrix Cracking	50-70	-	-	
			Debonding	60-80	-	-	
Carbon Fiber/ PEI	3PT Bending	-	Skin/Matrix Cracks	38-50	-	-	[71]
			Debonding	50-99	-	-	
Glass Fiber/Balsa	4PT Bending	K-means	Core Damage	Below 50	-	200-600	[72]
			Debonding	Below 50	-	80-400	
			Matrix Cracking	Below 51	-	20-200	
			Delamination	Above 70	-	20-200	
Glass Fiber/PVC Foam	Indentation Test	K-means++	Debonding	-	-	180-315	[61]
			Matrix Cracking	-	-	60-140	
			Fiber Breakage	-	-	360-453	
Carbon Fiber/ CNT-PU	3PT Bending	K-means genetic	Core Damage	40-87	-	400-750	[73]
			Debonding	40-98	-	270-400	
			Matrix Cracking	40-97	-	170-270	
			Fiber Breakage	40-99	-	0-170	
Glass Fiber/ Honeycomb	3PT Bending	K-means++	Core Damage	-	-	300-500	[74]
			Debonding	-	-	70-250	
			Matrix Cracking	-	-	0-70	
			Fiber Breakage	-	-	0-120	

1.3 Thesis Overview

In the literature review, it is seen that there are several studies on AE analysis of honeycomb- and foam-cored sandwich composites, but not much research has been done on nanomaterial-reinforced foam-cored sandwich composites. Within the scope of this thesis, using the AE test system, how the damage mechanisms of CNT/CNC-reinforced foam-cored sandwich composites were affected by the reinforcement studies was investigated. Damage mechanisms were classified using peak frequency, amplitude, and cumulative energy of AE data by the k-means genetic algorithm. In addition, as a subsection, the flexural performance of CNT-reinforced PU foam-filled 3D woven I-beam composites was studied. Thus, a preliminary study was carried out for CNT reinforcement studies on PU foam and its integration with sandwich composites. Furthermore, this preliminary study was meaningful for understanding the effect of PU foam usage on maintaining structural integrity and averting damage mechanisms in composite structures.

2. MATERIALS AND METHODS

2.1 Materials

The raw materials for the foaming process, Polyol 9022/100 and polymeric diphenylmethane diisocyanate (PMDI) were purchased from Aktif Poliüretan, Türkiye. 92% pure multi-walled CNTs having 8-10 nm diameter were acquired from Nanografi, Istanbul. CNCs were bought from Celluforce, Canada, and had dimensions of 2.3–4.5 nm in diameter and 44–108 nm in length. Sandwich composite face sheets were manufactured using four-plies unidirectional carbon fiber prepregs oriented 0/90/0/90. 600 TEX E-glass fibers with a 16 µm fiber diameter were purchased from Şişecam, Istanbul. The Hexion MGS L160 epoxy resin, with a viscosity and density of 700–900 mPas and 1.13–1.17 g/cm^3 at 25 °C, and the Hexion MGS H160 curing agent were both acquired from Dostkimya, Istanbul.

2.2 Manufacturing of PU Foam-Filled 3D Woven I-Beam Composites

600 TEX E-glass fibers were used to manufacture the 3D woven I beam, where TEX represents the mass of a 1000-meter-long fiber in grams. The 3D geometry was achieved using a 2D weaving machine by utilizing the weaving plan known as "Load Bearing X Vertical Wall" (LBX) depicted in Figure 2.1a. Whereas the dots in the weaving plan represent weft yarns, the green, blue, purple, and orange lines represent warp yarns, which come from the first weaver beam to form the web section. To create the 3-D geometry, two warp beams were utilized because the fabric had two warp layers with different lengths [75]. The web length and flange width were obtained as 2 cm and 16 cm, respectively. The vacuum-assisted resin transfer molding method (VARTM) was applied to manufacture I-beam composites as shown in Figure 2.1b. During the VARTM process, epoxy resin and curing agent were mixed in an 80:20 weight ratio. Peel ply and mesh were precisely placed both below and above the I-beam fabrics to simplify the demolding process and ensure optimal distribution of

epoxy. Teflon-coated molds were inserted into the space between the web and flanges of the I-beam to maintain the shape of the model.

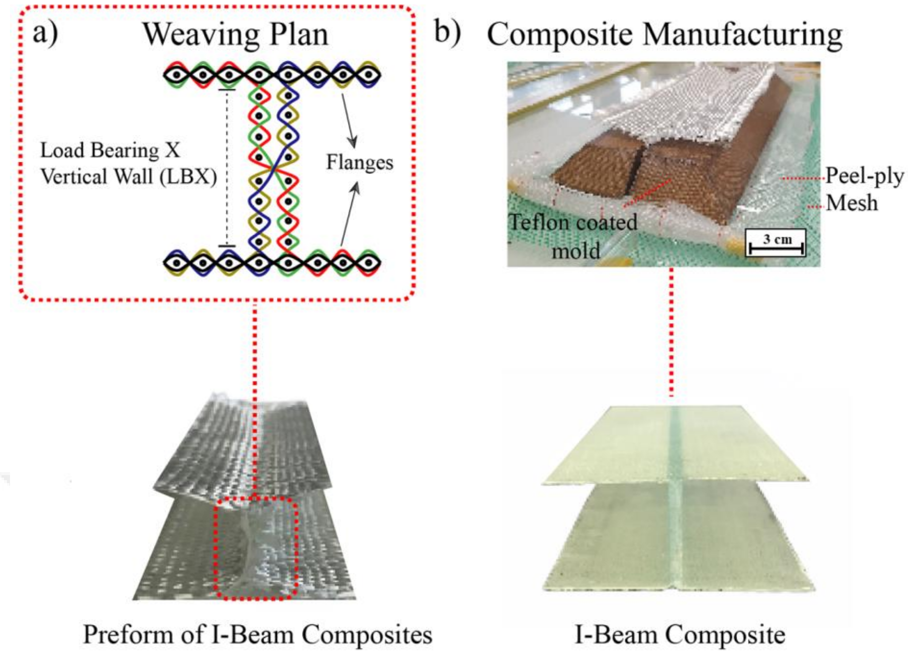

Figure 2.1 : An illustration of the a) weaving plan, and the composite manufacturing of b) I-beam composites.

2.2.1 PU foaming in I-beam composites

Manufacturing process of PU foams is generally initiated by mixing polyol and isocyanate for a certain time and ratio. Polyol contains catalysts, blowing agents, stabilizers, and curing agents. Polyols are organic chemical molecules containing multiple hydroxyl (OH) groups. Polyol and PMDI polymerization starts when the OH groups react with isocyanate (NCO) groups, forming a polymer with monomer units linked by urethane linkages [76].

The usual technique of pouring PU foam into a mold and then inserting it after adjusting its size to the desired dimensions was not used in this work. Instead, the foaming process of the PU foam was directly carried out in the vacancies between web and flanges of I-beam composite, without any adhesives. The manufacturer's manual recommends that the polyol and PMDI should be mixed at a speed of 2100 rpm for 40 seconds, using a weight ratio of 50:50 for the neat PU foam. Subsequently, a mixture of polyol and PMDI was poured into the vacancy between the web and flanges as illustrated in Figure 2.2a [75]. Afterwards, the specimen was inverted, and the remaining section was filled through the same foaming process. Then, the foam-filled

I-beam sandwich composite was placed in a 40 °C oven for 10 hours to stabilize and maintain the ambient temperature for the entire foaming period. In the case of CNT reinforcement, before mixing with polyol, CNTs were initially sonicated with PMDI for 5 minutes at 30% amplitude inside a beaker which is covered by ice cubes to prevent excessive heating. The final product of vacant, neat foam-filled, and CNT-reinforced foam-filled I-beam composites, after being cut into desired dimensions by compound miter saw, are shown in Figures 2.2b, 2.2c, and 2.2d, respectively.

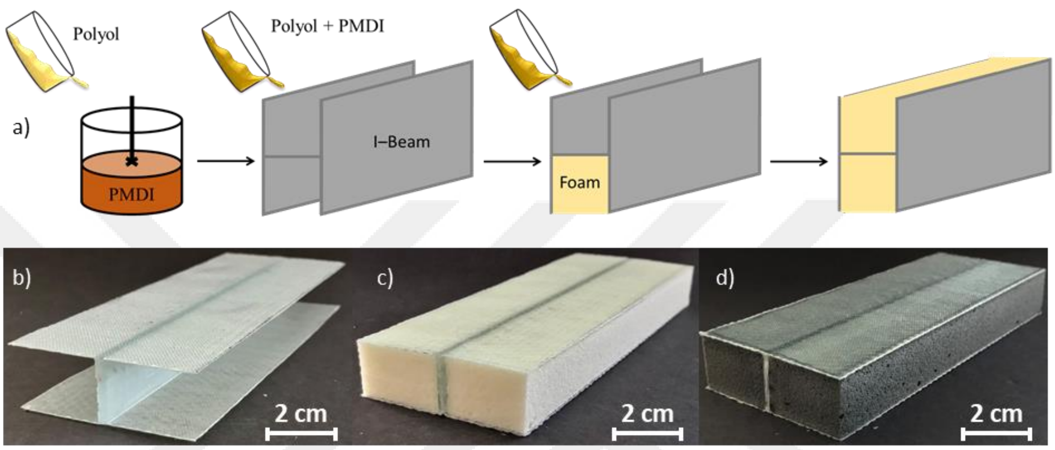

Figure 2.2 : Illustration of a) direct PU foaming method, and final products of b) vacant, c) neat, and c) CNT-reinforced PU foam-filled I-beams [75].

2.2.2 Compression tests of neat and CNT-reinforced PU foams

PU foams that directly foamed within the vacancies of I beams were manufactured in aluminum molds to investigate the increase in the material properties of neat PU foams by CNT reinforcement. A Shimadzu universal testing machine (UTM) with a 50 kN load cell was utilized to conduct compression tests on PU foams according to ASTM C365 standards with a 0.5 mm/min test speed. At least 5 test specimens were precisely cut to dimensions of 30x30x15 mm^3.

2.2.3 Three-point bending tests of 3D woven I-beam composites

The present study utilized the ASTM C393 standard, which is designed for sandwich composites, due to the absence of a corresponding standard specifically designed for three-point bending tests of 3D woven I-beam composites. The three-point bending test specimens shown in Figure 2.3 were prepared as 140x50x20 mm^3 for both vacant and foam-filled I-beam composites. The test apparatus of UTM with a 50 kN load cell had a span length of 90 mm. The test speed was set as 6 mm/min.

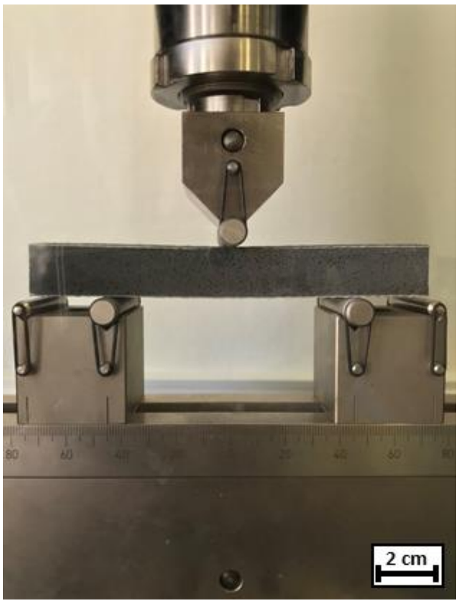

Figure 2.3 : Three-point bending test specimens of foam-filled I-beam composites.

2.3 Manufacturing of CNT/CNC-Reinforced PU Foam-Cored Sandwich Composites

For hybrid nano reinforcement studies, firstly, CNT/CNC dispersion in distilled water was prepared. Moreover, after the evaporation of distilled water, the hybrid nanomaterial was reinforced into the PU foam. After that, the necessary characterization studies were carried out.

2.3.1 CNT/CNC dispersion procedure

The CNT/CNC dispersion procedure begins with sonicating CNCs in distilled water as shown in Figure 2.4 for 8 minutes using a microtip sonicator at 20% amplitude and 10 Watts. Following that, CNTs were added to the distilled water/CNC dispersion. The same sonication technique was utilized this time, along with an ice cube treatment surrounding the beaker to prevent overheating. Subsequently, a petri dish containing distilled water/CNC/CNT dispersion, and 250 mbar was placed in an oven to dry for six hours under 250 mbar. Then, a pestle and mortar were used to grind the dried CNT/CNC to obtain powder form.

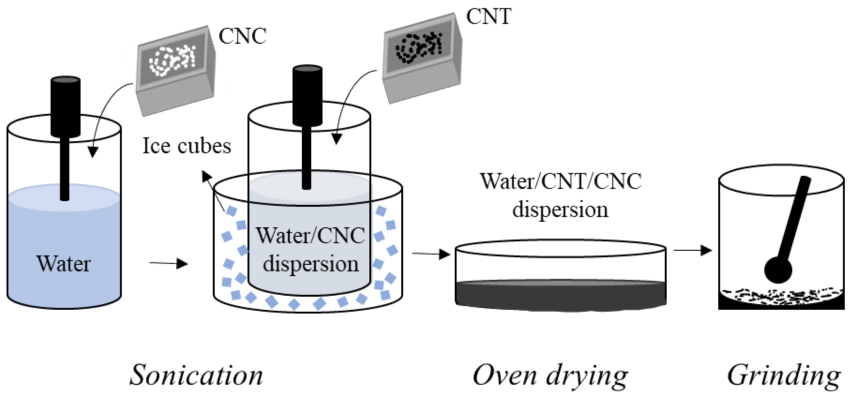

Figure 2.4 : CNT/CNC dispersion procedure in distilled water.

2.3.2 CNT/CNC-reinforced PU foaming procedure

The manufacturing process of CNT/CNC reinforced PU foam commences with the dispersion of PMDI and nanomaterials using a homogenizer operating at 10000 rpm for 7.5 minutes, as depicted in Figure 2.5. Then, polyol and PMDI/nanomaterial (1:1 weight ratio) were mixed with a mechanical stirrer for 40 seconds at 2100 rpm and poured into an aluminum mold. After 10 minutes of free-rise foaming at room temperature, the foam was placed in an oven at 40 °C for 10 hours in order to maintain a stable temperature during the foaming process.

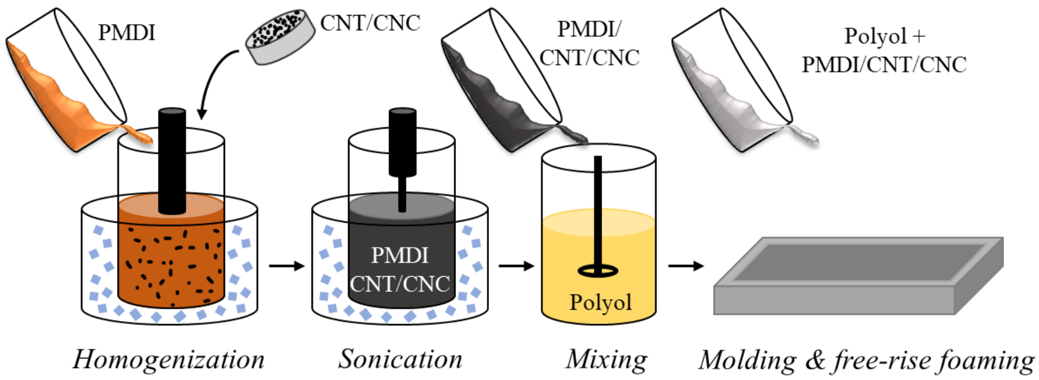

Figure 2.5 : Foaming of neat and nano-reinforced PU foams including homogenization, sonication, mixing, and molding procedures.

2.3.3 Morphological characterization

The scanning electron microscopy (SEM) technique was used to investigate the morphological properties of both neat and nano-reinforced PU foams. Prior to the imaging procedure, the samples were coated with a thin layer of gold in order to prevent surface charging. The SEM images were acquired under conditions of high vacuum and an accelerating voltage of 15 kV. The dimensions of cell edges (l), cell wall thicknesses (t), and cell densities (N) of both neat and nano-reinforced foams were measured and analyzed to evaluate the relationship between the microstructure and material properties of PU foams.

2.3.4 Compression tests of CNT/CNC PU foams

The compression tests of PU foams were conducted using a Shimadzu UTM, as shown in Figure 2.6, equipped with a 50 kN load cell. The tests were carried out following the guidelines specified in ASTM C365-16 standards. The test specimens were precisely cut to dimensions of 30x30x15 mm^3. At least 5 specimens were subjected to testing with a test speed of 0.5 mm/min.

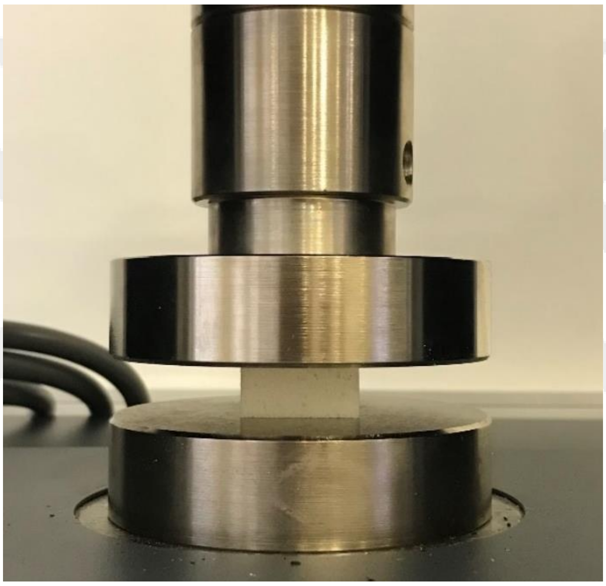

Figure 2.6 : Compression test of neat and CNT/CNC-reinforced PU foams.

2.3.5 Three-point bending and AE tests of sandwich composites

Three-point bending tests were conducted using computer controlled Instron 8872 UTM, adhering to ASTM C393 standards. The tests were performed at a crosshead speed of 2 mm/min, and the machine had a load cell capacity of 10 kN. The core material was trimmed to dimensions of 150x50x15 mm^3, and a total of 3 sandwich composite test specimens were tested for each type. Two AE sensors were positioned 100 mm apart on either side of the specimen to observe and track instances of damage. A PCI-2 AE data acquisition system (PAC) with a maximum sampling rate of 40 MHz was utilized to capture the AE signals. PAC broadband implemented AE sensors using single-crystal piezoelectric transducers. The sensors operated within a frequency range of 100–1000 kHz, while the preamplifier's threshold and maximum value were 40 dB and 99 dB, respectively. The sensor's surface was coated with silicon grease to ensure effective acoustic coupling between the specimen and the sensor. The sampling rate for the test was 5 MHz. The calibration of the data acquisition system for each specimen was performed using a pencil lead break procedure. Following the calibration process, the AE signals were recorded during the three-point bending tests, as shown in Figure 2.7.

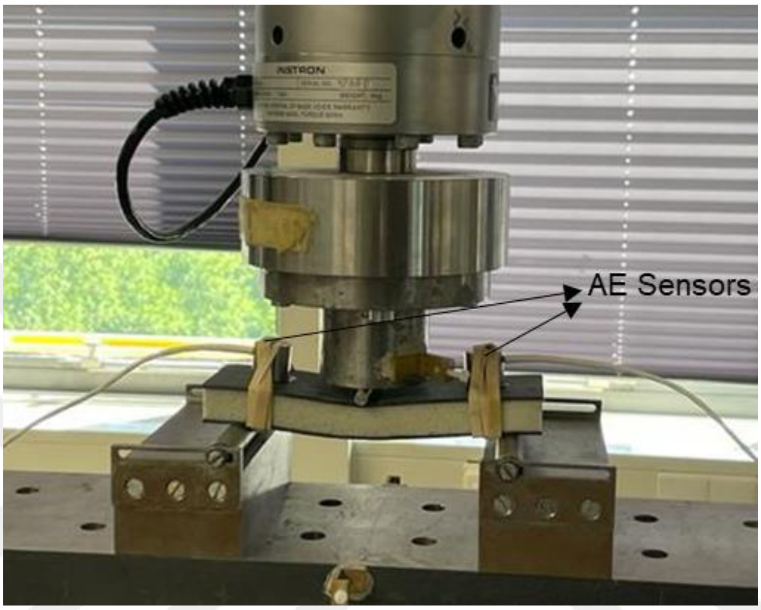

Figure 2.7 : AE sensors connected to the sandwich composites during a three-point bending test.

3. RESULTS AND DISCUSSION

This section contains two subsections: flexural response of PU foam-filled 3D woven I-beam composites and damage detection of PU foam-cored sandwich structures. In the first subsection, compression test results of neat and 0.1 wt.% CNT-reinforced PU foams and the three-point bending test results of neat and 0.1 wt.% CNT-reinforced PU foam-filled I-beam composites were investigated. The effect of the strengthened core material with CNT reinforcement on the flexural performance of foam-filled I-beam composites was discussed. In the second subsection, neat and CNT/CNC-reinforced PU foam's morphological analysis, with a discussion of the findings regarding microstructure and mechanical properties was presented. Afterwards, the compressive test results of PU foams, three-point bending and simultaneous AE test of sandwich composites were analyzed. The AE data was investigated in conjunction with the three-point bending results to identify the damage mechanisms of foam-cored sandwich composites. The outcomes were evaluated, and the influence of nanomaterial reinforcements on the damage mechanisms was discussed.

3.1 Flexural Response of PU Foam-Filled 3D Woven I-Beam Composites

3.1.1 Compression test of neat and CNT-reinforced PU foams

Compression tests of neat PU (N-PU) and 0.1 CNT-reinforced PU (0.1CNT-PU) foams were performed to investigate how CNT reinforcement affects the compressive properties of PU foams. The densities of N-PU and 0.1CNT-PU foams were calculated as 111.71±1.66 kg/m^3 and 112.95±1.05 kg/m^3, respectively, before conducting compression tests. The CNT reinforcement is assumed to cause smaller cell sizes and thicker cell walls in the morphological characteristics of N-PU foams. However, a verification process such as SEM imaging is necessary to confirm this claim. This subsection does not address the SEM image process; however, it is discussed in the second subsection.

The compression test results, obtained as load and displacement data, were transformed into stress and strain data using equations 3.1 and 3.2, plotted in Figure 3.1. CNT reinforcement does not significantly affect the compressive strength, as revealed by the values of 1.06±0.04 MPa and 1.10±0.03 MPa for N-PU and 0.1CNT-PU, respectively. On the other hand, the compressive modulus of N-PU and 0.1CNT-PU were calculated as 26.08±1.80 MPa and 30.63±2.11 MPa, respectively. Compression test results of each test specimen can be found in Table A.1. CNT reinforcement remarkably increased the stiffness of N-PU, resulting in a 14.23% increase in compressive modulus. Therefore, 0.1CNT-PU was considerably stronger as a core material of sandwich composites and filler of I-beam composites than N-PUs.

$$\sigma_c = \frac{P}{A} \tag{3.1}$$

$$\epsilon_c = \frac{h}{h_0} \tag{3.2}$$

where σc is the compressive stress, P is the load, A is the cross-section area, ϵ_c is the compressive strain, h is the stroke and h_0 is the initial height of the test specimen.

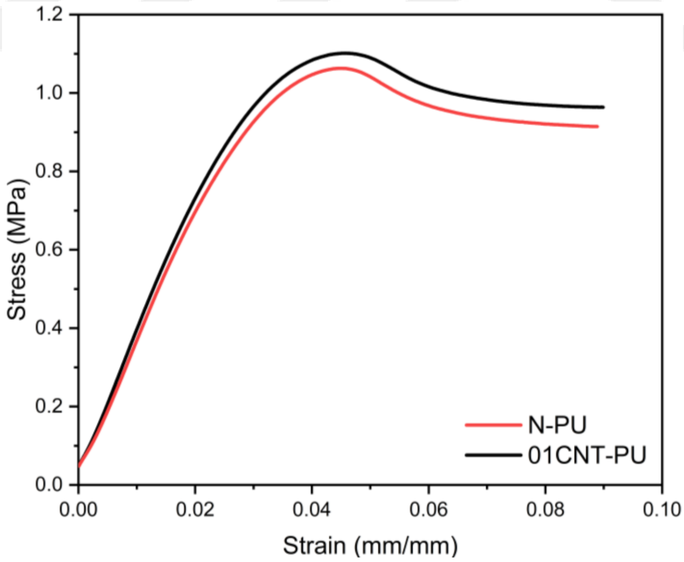

Figure 3.1 : Representative compressive stress-strain data of N-PU and 0.1CNT-PU foams.

3.1.2 Three-point bending tests of I-beam composites

Flexural properties and the structural integrity of the hollow (H-LBX), N-PU foam-filled (N-PU-LBX), and 0.1CNT-PU foam-filled (0.1CNT-PU-LBX) I-beam composites were evaluated through three-point bending tests to assess the impact of direct PU foaming. Moreover, the effect of strengthened core material by CNT reinforcement on the flexural response of foam-filled I beams was investigated as well. The load-bearing capacities of I-beam composites were determined utilizing force and displacement data, while stress and strain curves were obtained for flexural modulus and flexural strength calculations using equations 3.3 and 3.4. Stress-strain data of H-LBX, N-PU-LBX, and 01CNT-PU-LBX under three-point bending tests were shown in Figure 3.2 and the flexural properties were summarized in Table 3.1. Three-point bending test results of each I-beam composite were given in Table A.2.

$$\sigma_f = \frac{3PL}{2bd^2} \tag{3.3}$$

$$\epsilon_f = \frac{6Dd}{L^2} \tag{3.4}$$

where σ_f is the flexural stress, P is the load, L is the support span, b is the width and d is the depth of the sandwich structure, ϵ_f is the flexural strain and D is the maximum deflection of the center of the beam.

Table 3.1 : Flexural properties of I-beam composites.

Specimen	Load Bearing Capacity (kN)	Increase (%)	Flexural Modulus (MPa)	Increase (%)	Flexural Strength (MPa)	Increase (%)
H-LBX	2.52±0.33	-	478.63±25.95	-	14.67±1.26	-
N-PU-LBX	3.46±0.30	53.70	629.81±49.39	31.59	22.77±2.32	55.18
01CNT-PU-LBX	3.54±0.49	57.00	670.32±56.40	40.05	23.07±2.84	57.23

The direct PU foaming method drastically improved the load-bearing capacity, flexural strength, and flexural modulus of H-LBX, as indicated by the outcomes of the three-point bending tests. Furthermore, Figure 3.2 illustrates that the addition of PU foam contributes to the linearity of the elastic region, which corresponds to approximately 3% strain. Thus, the structural integrity of H-LBX was enhanced, resulting in an expanded linear elastic region and increased resistance to cyclic loads at low strain levels. Moreover, load bearing capacity, flexural modulus, and flexural strength of N-PU-LBX were increased in 01CNT-PU-LBX by 6.15%, 26.78%, and 3.72%, respectively. Hence, these findings are deemed highly encouraging, as higher concentrations of CNTs can lead to significant enhancements in mechanical properties without incurring a substantial increase in weight. Moreover, the enhancements in the load bearing capacity and flexural strength a slightly different due to the challenge of cutting same-sized specimens by miter saw.

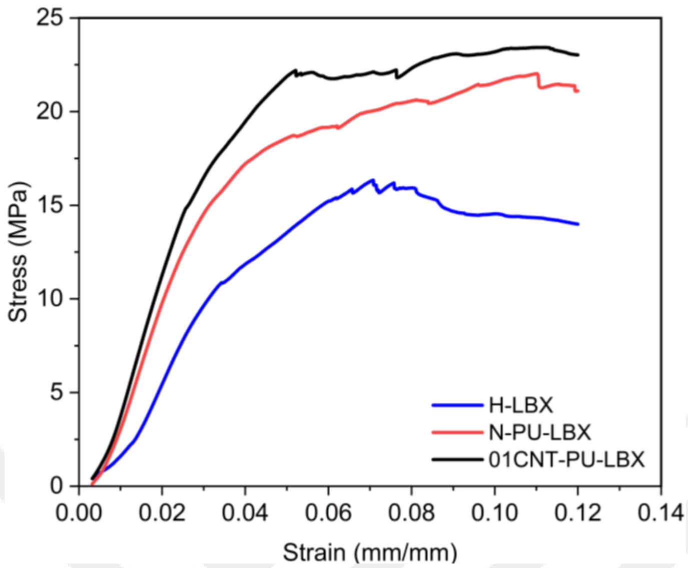

Figure 3.2 : Representative stress-strain curves of H-LBX, N-PU-LBX, and 01CNT-PU-LBX under three-point bending tests.

Besides increasing flexural properties, maintaining structural integrity is another case study to be considered to design reliable 3D woven I-beam composites. Thin-walled I-beam composites are prone to twist under high loading conditions as demonstrated in Figure 3.3a. Assembling ribs into the space between the web and flanges could potentially prevent twisting. However, this approach may introduce further complications, such as the necessity of developing a suitable joint design between the ribs and I-beam, the possibility of cracks emerging at the joints, or the requirement for a new weaving design of 3D woven composites. Hence, the direct foaming between the web and flanges could be a simple and effective approach to overcome twisting and torsional buckling, as shown in Figure 3.3b. As a result, direct foaming between the web and flanges effectively mitigates any concerns regarding the torsional behavior of I-beams under high loadings.

On the other hand, when foam is added, new failure mechanisms show up at high loads, such as the indentation of the load pin into the test specimen and debonding, as shown in Figures 3.3b and 3.3c. Indentation in H-LBX was observed at low loadings due to the change in a substantial proportion of the flexural stress into shear stress induced by twisting. Furthermore, the foam-filled sandwich composite shown in Figure 3.3c has suffered from debonding instead of indentation at a similar loading as given in Figure 3.3b. The absence of adhesive bonding between the foam and the beam has been predicted as a reason for this damage mechanism under high load conditions. Moreover, Figure 3.3d demonstrates that during failure, the beam exhibits cracks at the central cross-section, precisely at the location where the bending moment reaches its maximum value. This behavior indicates that the dominant loading type became bending while the effects of other types were resisted.

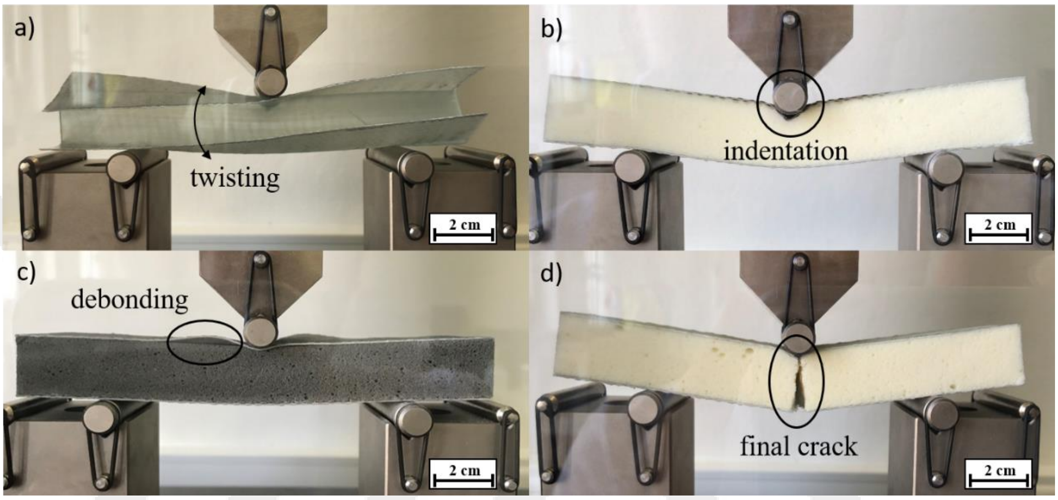

Figure 3.3 : Detection of a) twisting, b) indentation, c) debonding, and d) core crack under three-point bending tests of I-beam composites.

3.2 Damage Detection of PU Foam-Cored Sandwich Structures

Morphological analysis were performed to investigate the effect of hybrid CNT/CNC reinforcement on the cell parameters and mechanical properties of neat PU foams. Moreover, compressive properties of PU foams were performed. Furthermore, three-point bending tests of foam-cored sandwich composites were performed simultaneously with acoustic emission testing.

3.2.1 SEM results

The representative SEM images at a magnification factor of 200x show sections of the neat and nano-reinforced PU foams, as shown in Figure 3.4a and 3.4b, respectively. These resulting images exhibit a distinct and uniform distribution of foam cells. The cell density (N) and the ratio of cell wall thickness (t) to edge length (l) which are indicated in Figures 3.4c and 3.4d, respectively, are significant variables in determining the enhancement of mechanical properties, particularly strength and elastic modulus. ImageJ software was utilized to analyze SEM results. The calculation of cell density was performed using equation 3.5 [15]. The cell sizes exhibited variations can be attributed to the heterogeneous nucleation mechanism of foams [7].

$$N = \left(\frac{nM^2}{A}\right)^{1.5} \tag{3.5}$$

where *N* is the cell density, *n* is the number of cells, *A* is the micrograph area, and *M* is the magnification factor.

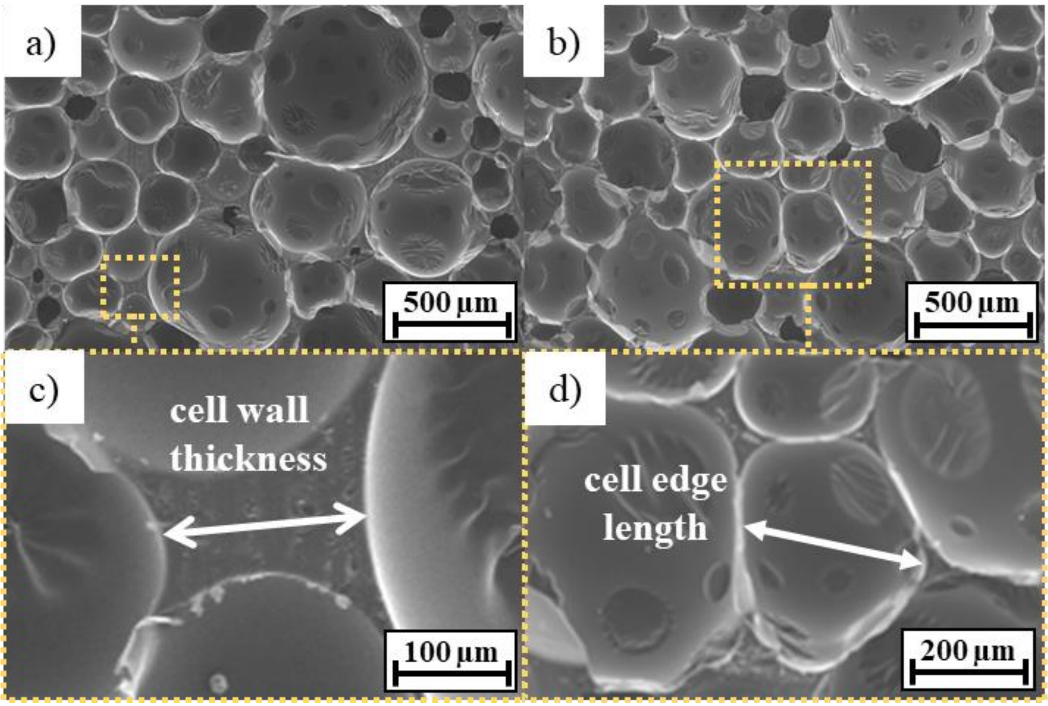

Figure 3.4 : Representative SEM images of a) neat and b) nano-reinforced PU foams, c) cell wall thickness, and d) cell edge length.

Table 3.2 presents a concise overview of the SEM results and morphological characteristics of PU foams. Samples of neat, 0.1 wt.% CNT, 0.1 wt.% CNC, 0.1 wt.% CNT/CNC (1:1), and 0.1 wt.% CNT/CNC (1:2) reinforced PU foams were categorized as N-PU, 0.1CNT-PU, 0.1CNC-PU, 0.1CNT/CNC(1:1)-PU, and 0.1CNT/CNC(1:2)-PU, respectively. The analysis and calculations revealed that the N-PU has a cell edge length of 103.98±8.47 µm, a cell wall thickness of 29.21±4.71 µm, a t/l ratio of 0.28, and a cell density of 2.65×10^4 cells/cm^3. As a result of the nanomaterial reinforcement, t, and l values were decreased. Whereas the t/l ratio and cell densities were both increased by 0.1% wt. CNT and 0.1% wt. CNC reinforcement, there was no significant change in the t/l ratio for 0.1% wt. CNT/CNC(1:1)-PU and 0.1% wt. CNT/CNC(1:2)-PU.

Table 3.2 : Overview of the SEM results and morphological characteristics of PU foams.

Specimen	Cell Edge Length (l) (µm)	Cell Wall Thickness (t) (µm)	t/l	Cell Density ($x10^4$ cells/cm^3)
N-PU	103.98±8.47	29.21±4.71	0.28	2.65
0.1CNT-PU	74.02±11.33	26.34±4.53	0.36	4.17
0.1CNC-PU	77.44±9.82	25.47±4.38	0.33	3.07
0.1CNT/CNC(1:1)-PU	86.79±11.25	23.32±4.00	0.27	3.43
0.1CNT/CNC(1:2)-PU	83.63±13.17	23.98±4.47	0.29	3.16

3.2.2 Compression test results of CNT/CNC-reinforced PU foams

Figure 3.5 displays the stress-strain data of compression test results of PU foams. Moreover, compression test results of each neat and CNT-, CNC-, and CNT/CNC-reinforced PU test specimens can be found in Table A.3. Density, compressive strength and compressive modulus of the neat PU foam were calculated as 111.25±0.16 kg/m^3, 0.99±0.01 MPa and 29.36±1.09 MPa, respectively, based on the stress-strain data provided.

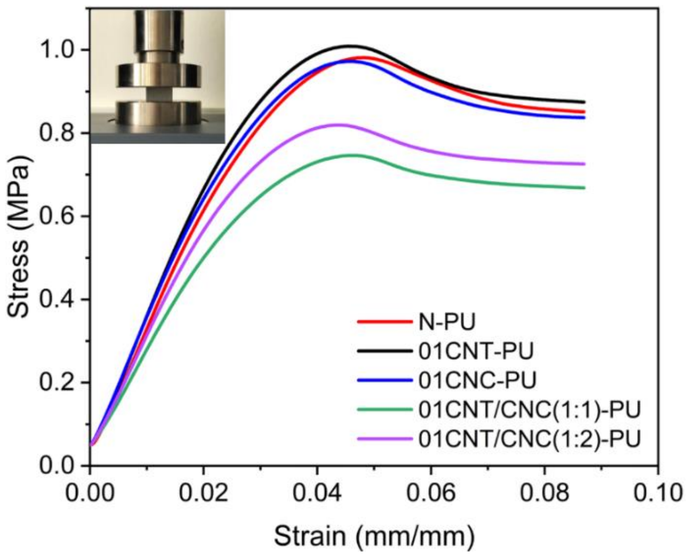

Figure 3.5 : Representative stress-strain curves of neat and CNT/CNC reinforced PU foams under compression tests.

The compression test results demonstrated that the reinforcement of nanomaterials did not yield any considerable improvement in compressive strength, regardless of the nanomaterial concentration. Nevertheless, 0.1 wt.% CNT and 0.1 wt.% CNC reinforcement increased the compressive modulus of the PU foams by 13.89% and 7.19%, respectively. In contrast, the 0.1 wt.% CNT/CNC(1:1) and 0.1 wt.% CNT/CNC(1:2) nanomaterial reinforcement resulted in a decrease of PU foams' compressive modulus by 15.21% and 2.87%, respectively. The fundamental reasons for this behavior can be attributed to the agglomerations of nanoparticles and the potential oversight of certain factors during the drying process of CNT/CNC dispersion.

3.2.3 Three-point bending test results of sandwich composites

Three-point bending test instrumentation and stress/strain data are shown in Figure 3.6. Three-point test specimens of sandwich composites having neat, 0.1 wt.% CNT, CNC, CNT/CNC (1:1), and CNT/CNC (1:2) reinforced PU foams as core material were named as N-PU, 0.1CNT-PU, 0.1CNC-PU, 0.1CNT/CNC(1:1)-PU, and 0.1CNT/CNC(1:2)-PU, respectively. Furthermore, three-point bending test results of each neat and CNT-, CNC-, and CNT/CNC-reinforced PU foam-cored sandwich composites were given in Table A.4.

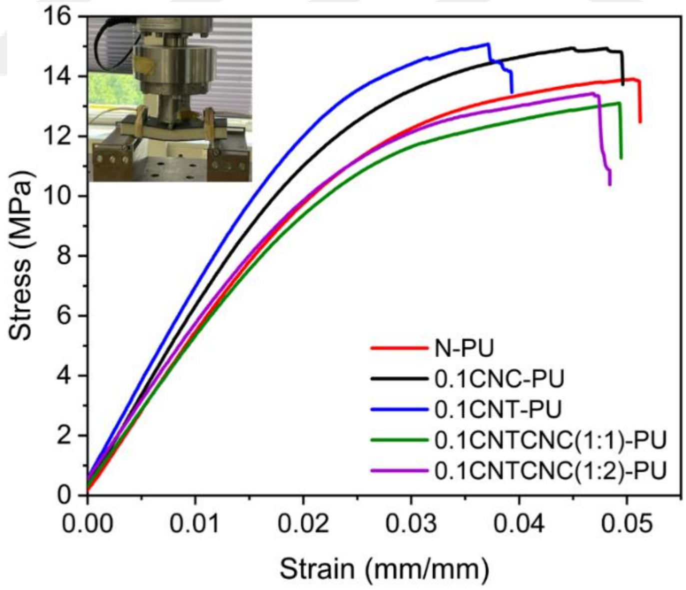

Figure 3.6 : Representative stress-strain curves of sandwich composites under three-point bending tests.

The flexural properties exhibited an adequate relationship with the compressive properties. The load-bearing capacity, flexural strength, and flexural modulus of neat PU foams were increased by 6.84%, 6.88%, and 16.03%, respectively, by 0.1 wt.% CNT-reinforced PU foam-cored sandwich composites. Moreover, the load-bearing capacity, flexural strength, and flexural modulus were enhanced by 7.55%, 7.07%, and 14.15%, respectively, with the 0.1 wt.% CNC reinforcement of neat PU foam. While the addition of individual 0.1 wt.% CNT and CNC reinforcements had a positive impact on the mechanical properties of neat PU foams, their combination did not meet the expectations. The combination of CNT and CNC through a hybrid reinforcement resulted in reduced mechanical properties in 0.1CNT/CNC(1:1)-PU and 0.1CNT/CNC(1:2)-PU samples. The hybrid reinforcement was anticipated to benefit from the bonding capabilities of CNC with CNTs in order to hinder the formation of strong van der Waals bonds between CNTs. Nevertheless, the hybridization led to inferior mechanical properties in 0.1CNT/CNC(1:1)-PU and 0.1CNT/CNC(1:2)-PU samples. Hence, the decrease in mechanical properties is primarily ascribed to the process of oven drying the CNT/CNC aqueous dispersion.

3.2.4 AE data analysis

By gathering AE data during the three-point bending test, individual data points can be identified and clustered to ascertain the type of damage they are associated with. The main parameters frequently used for interpreting the AE data are amplitude, peak frequency, energy, signal duration, and rise time, as extensively documented in the literature. Nevertheless, signals associated with distinct types of damage may exhibit parallel amplitude and energy levels, resulting in overlapping regions that are difficult to classify. In order to tackle this issue, prior research [63,69,77] has demonstrated that utilizing peak frequency data is an optimal approach for clustering and leads to a more precise categorization of damage mechanisms. The cumulative energy data strongly affects the determination of which cluster belongs to which damage mechanism. Hence, the AE characteristics of the specimens were analyzed using parameters such as peak frequency, amplitude, energy, cumulative energy, and the number of AE hits. Graphs depicting the relationship between peak frequency and amplitude (Fig. 3.7a), load-energy and displacement (Fig. 3.7b), and load-cumulative energy and displacement (Fig. 3.7c) were plotted for every test specimen. The k-means genetic algorithm was subsequently employed to improve both the accuracy and dependability of the damage classification.

Four clusters were created similar to prior research conducted on sandwich composites [39,63,67,69,74]. Each of these four clusters represents a distinct damage type, including core damage, core-face sheet debonding, matrix cracking, and fiber breakage. Core damage includes both PU foams and reinforcement materials, whereas matrix cracking and fiber breakage specifically denote the failures of epoxy resin and carbon fibers in laminated face sheets. AE signal clustering can be performed by taking into account the corresponding peak frequency and amplitude data, as depicted in Figure 3.8. Since the mechanical properties of neat PU foams were only increased by 0.1 wt.% CNT, and 0.1 wt.% CNC reinforcement, the AE characteristics such as peak frequency, and amplitude data were only shown for N-PU, 0.1CNT-PU, and 0.1CNC-PU in Figures 3.8a, 3.8b, and 3.8c, respectively. On the other hand, even tough the graphs including AE hits belong to the 0.1CNT/CNC(1:1)-PU and 0.1CNT/CNC(1:2)-PU samples were not plotted, their AE data were used to classify damage modes to assess the clasification of AE hits into proper clusters for comparison.

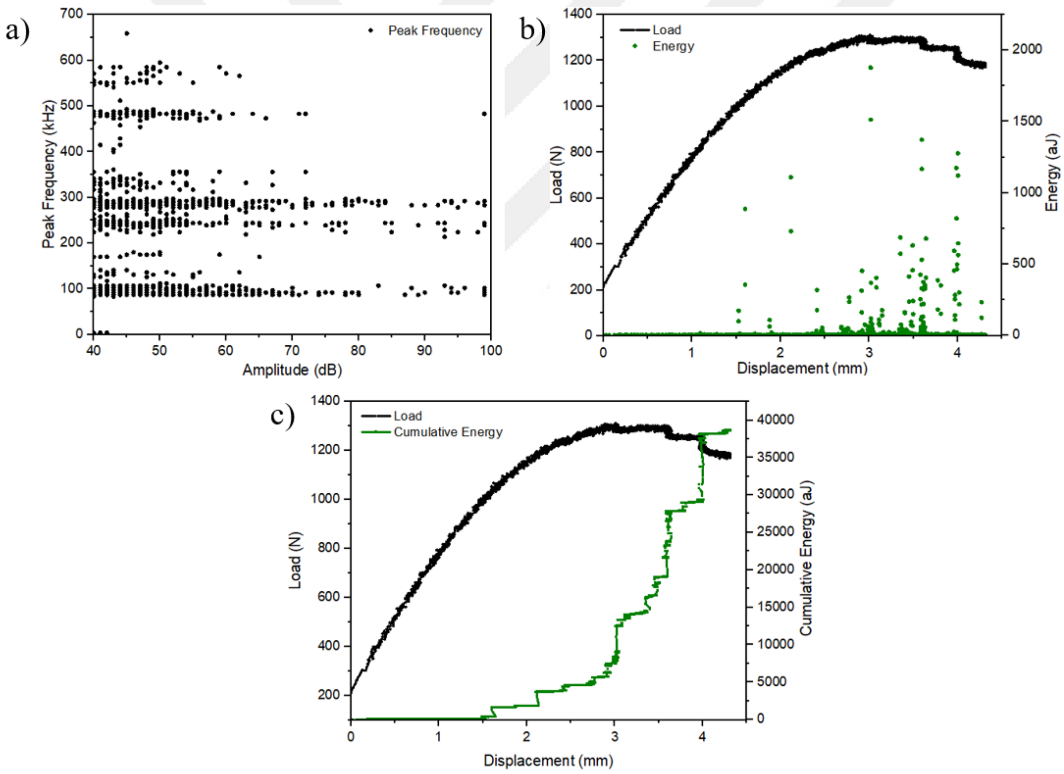

Figure 3.7 : Representative graphs of a) peak frequency vs. amplitude b) load-energy vs. displacement, and c) load-cumulative energy vs. displacement.

Solely considering the amplitude range is inadequate for partitioning AE data into clusters. However, when the peak frequency is considered with the amplitude range, clusters can be effectively separated. The AE clusters were classified based on peak frequency-amplitude data and represented by distinct colors, including blue, green, purple, and red. Furthermore, by analyzing Fig. 3.8 and the load-cumulative energy vs. displacement curves, four damage types were identified and categorized in Table 3.3. These damage types are listed in ascending order of frequency, including fiber breakage, matrix cracking, face sheet-core debonding, and core damage.

Table 3.3 : Summary of damage classification according to frequency ranges.

Damage Type	Frequency Range (kHz)
Core Damage	400-750
Debonding	270-400
Matrix Cracking	170-270
Fiber Breakage	0-170

In the literature, AE test analyses reveal that different types of damage mechanisms result in distinct AE signals for composite structures. For example, matrix cracking can generally be characterized by low amplitude and frequency, long duration, and long rise time. On the other hand, delamination is characterized by medium amplitude, low frequency, and very long duration. It is commonly observed that fiber breakage in face sheets of sandwich composites and laminated composites is associated with high-frequency values in the acquired AE data [39,67,69]. However, there are contradicting results from other studies that suggest the opposite [74,78]. The variation in frequency outputs of the studies may be attributed to specimen types, such as laminated composites and sandwich composites, as well as the testing methods employed, such as tensile, DCB, and three-point bending. The study utilized the AE test to evaluate the foam-cored sandwich composites during a three-point bending test conducted simultaneously. The AE characteristics are unique for this test setup because this content has not been studied in previous research in literature.

Figure 3.8d shows the relationship between load and displacement, demonstrating the cumulative energy associated with different damage types. Since being the strongest material in the test specimen, the AE data recorded at the final failure throughout the three-point bending tests were classified as fiber breakage events that have high energy release by each AE hits. The matrix cracking damages were identified by analyzing the AE hits, which are simultaneous but have a lower cumulative energy compared to fiber breakage, contributing to the final failure. The main difference between matrix cracking and debonding is that while the cumulative energy of matrix cracking is more progressive, debonding has sharper energy releases that happen due to the rapid failure of the bond between the core and the face sheets. Furthermore, it was determined that the occurrence of high-frequency, low-energy AE hits during the initial stages of the three-point bending test leads to core damage. Moreover, the core material, which is the weakest material in the sandwich composite test specimen, experiences crushings that cause the lowest energy releases instead of cracking until the final failure. Furthermore, Figure 3.8 demonstrates that the distribution of AE hits is more closely grouped for debonding in both 0.1CNT-PU and 0.1CNC- compared to N-PU. In addition, AE data related to core damage in 0.1CNT-PU and matrix cracking data in 0.1CNC-PU were collected within a narrow frequency range.

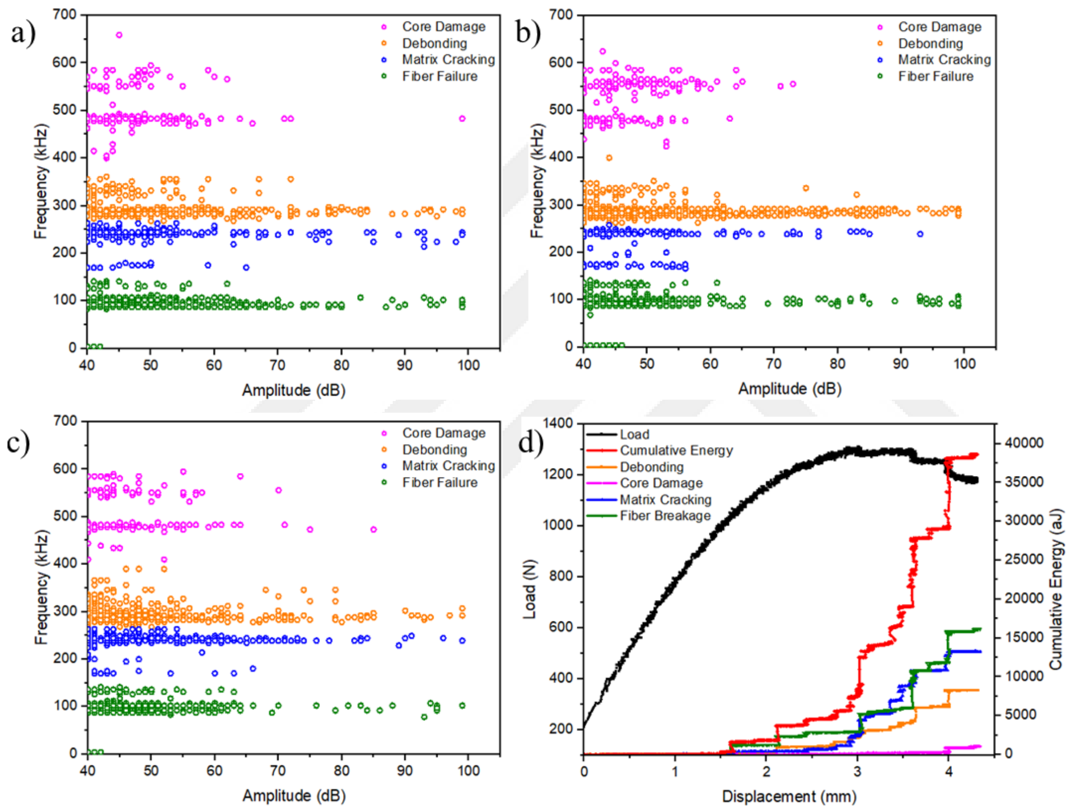

Figure 3.8 : Peak frequency/Amplitude data of a) N-PU, b) 0.1CNT-PU, c) 0.1CNC-PU, and d) representative cumulative energy data of separate damage mechanisms.

The prevalence of failure mechanisms can be quantified by examining the amount and energy of AE hits. Table 3.4 displays the proportion of AE hits recorded until failure and Table 3.5 shows the cumulative energy for each damage mechanism. Due to the prior failure of the sandwich material having weaker core material, Table 3.4 demonstrates that the reinforced sandwich composites, except for 0.1 wt.% CNT and 0.1 wt.% CNC, have a higher fiber breakage ratio. Reinforcing 0.1 wt.% CNT and 0.1 wt.% CNC to the core materials enhances their strength. This results in an increased loading endurance between the face sheets and a decreased overall fiber breakage ratio.

Furthermore, Table 3.5 demonstrates that the cumulative energy data related to core damage and fiber breakage were decreased by a factor of six and nearly two, respectively, with 0.1 wt.% CNT reinforcement of PU foam. As a result, the ideal concentration of nanomaterials for supporting the face sheets under flexural loads and fortifying the core material is determined to be 0.1 wt.% CNT.

Table 3.4 : Number of AE hits dominance of each damage mechanism.

Damage Type	N -PU	0.1CNT -PU	0.1CNC -PU	0.1CNT/CNC (1:1)-PU	0.1CNT/CNC (1:2)-PU
Core Damage	7.37%	6.64%	10.76%	9.99%	7.08%
Debonding	25.82%	32.82%	25.93%	14.06%	23.14%
Matrix Cracking	25.25%	24.68%	25.77%	17.38%	21.59%
Fiber Breakage	41.56%	35.86%	37.54%	58.57%	48.19%

Table 3.5 : Cumulative energy dominance of each damage mechanism.

Damage Type	N -PU	0.1CNT -PU	0.1CNC -PU	0.1CNT/CNC (1:1)-PU	0.1CNT/CNC (1:2)-PU
Core Damage	3.05%	0.51%	1.28%	3.97%	0.78%
Debonding	11.74%	43.61%	22.26%	17.73%	28.30%
Matrix Cracking	20.85%	18.22%	27.27%	10.78%	11.20%
Fiber Breakage	64.36%	37.66%	49.19%	67.52%	59.72%

4. CONCLUSION

In this study, PU foam cores of sandwich composites were reinforced with 0.1 wt.% CNT, CNC, CNT/CNC (1:1), and CNT/CNC (1:2) nanomaterials. Moreover, before starting CNT/CNC hybridization, PU foams were solely reinforced with 0.1 wt.% CNT and directly foamed within the unit cells of 3D woven I-beams composites as a subsection. The effect of PU foaming on the structural integrity of I-beam composites was investigated and the contribution of CNT nano reinforcement in the flexural properties of neat foam-filled I-beam composites was analyzed.

In the first subsection, it is found that the direct PU foaming within the vacancies of 3D woven I-beam composites suppressed the twisting and torsional buckling of vacant I-beam composites under high loadings. Thus, structural integrity was maintained and more reliable I-beam composites were manufactured. Moreover, 0.1 wt.% CNT reinforcement of neat PU foams in I-beam composites resulted in an increase in flexural properties without any significant weight penalty.

In the second subsection, the study involved reinforcing processes of PU foam cores with 0.1 wt.% of CNT, CNC, CNT/CNC in a 1:1 ratio and CNT/CNC in a 1:2 ratio. The main focus of the study was to enhance the strength of the PU foam core by increasing the concentration of CNTs and preventing agglomeration by incorporating CNC as an additional nanomaterial reinforcement. The investigation also considered the chemical compatibility of these materials and their dispersion in water. The foam-cored sandwich composites were tested under simultaneous three-point bending and AE tests to investigate the impact on their mechanical properties and damage mechanisms. While 0.1 wt.% CNT and CNC reinforcement of the core improved its mechanical properties, with the addition of 0.1 wt.% CNT demonstrated the most successful results in terms of both compression and flexural response. Additionally, SEM images demonstrated that the improvements in compressive and bending properties were justified by increases in the ratio of cell edge length to wall thickness and cell density through nano reinforcement with 0.1% wt. CNT and 0.1% wt. CNC. Moreover, the analysis of the AE data with the k-means genetic algorithm enabled a categorization of damage mechanisms during three-point bending tests. The results gathered from the AE hits dominance analysis indicate that the addition of nanomaterials at a concentration as low as 0.1 wt.% can effectively reduce core damage and fiber breakage by strengthening the core.

The decrease in the mechanical properties of neat PU foams reinforced with CNT/CNC hybrid systems can be attributed to the drying method of CNT/CNC dispersion employed in this study. The attainment of nanoparticles with uniform sizes and ensuring the consistency of the process are two crucial challenges that require solving in the oven drying and grinding methods. Consequently, freeze-drying can be employed as a dependable alternative technique to maintain the nanoscale dimensions of the particles in a future study. Hence, one can attain a drying process that is more reliable and consistent by sublimating the distilled water from the dispersion of CNT/CNC/distilled water.

REFERENCES

[1] **Federal Aviation Administration** (2016). Pilot's handbook of aeronautical knowledge: FAA-H- 8083-25B. *Chapter 10: Weight and Balance*. Newcastle: Aviation Supplies & Academics.

[2] **Singh, J., Sharma, S. K., & Srivastava, R.** (2019). What drives Indian Airlines operational expense: An econometric model. *Journal of Air Transport Management, 77,* 32-38.

[3] **Mansor, M. R., Nurfaizey, A. H., Tamaldin, N., & Nordin, M. N. A.** (2019). Natural fiber polymer composites: Utilization in aerospace engineering. In Biomass, biopolymer-based materials, and bioenergy (pp. 203-224). *Woodhead Publishing.*

[4] **Irving, P. E., & Soutis, C**. (2019). Polymer composites in the aerospace industry. *Woodhead Publishing.*

[5] **Piquet, B.** (2013). Special Edition A350XWB, *FAST (Flight Airworthiness Support Technology) - Airbus Technical Magazine.*

[6] **Vinson, J. R.** (2005). Sandwich structures: past, present, and future. In Sandwich Structures 7: Advancing with Sandwich Structures and Materials: *Proceedings of the 7th International Conference on Sandwich Structures,* Aalborg University, Aalborg, Denmark, 29–31 August 2005 (pp. 3-12). Springer Netherlands.

[7] **Caglayan, C., Gurkan, I., Gungor, S., & Cebeci, H.** (2018). The effect of CNT-reinforced polyurethane foam cores to flexural properties of sandwich composites. *Composites Part A: Applied Science and Manufacturing, 115,* 187-195.

[8] **Schubel, P. M., Luo, J. J., & Daniel, I. M.** (2007). Impact and post impact behavior of composite sandwich panels. *Composites Part A: applied science and manufacturing, 38(3),* 1051-1057.

[9] **Herrmann, A. S., Zahlen, P. C., & Zuardy, I.** (2005). Sandwich structures technology in commercial aviation: Present applications and future trends. In Sandwich Structures 7: Advancing with Sandwich Structures and Materials: *Proceedings of the 7th International Conference on Sandwich Structures,* Aalborg University, Aalborg, Denmark, 29–31 August 2005 (pp. 13-26). *Springer Netherlands.*

[10] **Zuardy, M. I., & Herrmann, A. S.** (2011). An advanced centre box of a vertical tail plane with a side panel from CFRP foam-core sandwich structure. *CEAS Aeronautical Journal, 2(1-4),* 253-269.

[11] **Kausar, A.** (2018). Polyurethane composite foams in high-performance applications: A review. *Polymer-Plastics Technology and Engineering, 57(4),* 346-369.

[12] **Ciecierska, E., Jurczyk-Kowalska, M., Bazarnik, P., Gloc, M., Kulesza, M., Kowalski, M., ... & Lewandowska, M.** (2016). Flammability, mechanical properties and structure of rigid polyurethane foams with different types of carbon reinforcing materials. *Composite Structures, 140,* 67-76.

[13] **Navidfar, A., Sancak, A., Yildirim, K. B., & Trabzon, L.** (2018). A study on polyurethane hybrid nanocomposite foams reinforced with multiwalled carbon nanotubes and silica nanoparticles. *Polymer-Plastics Technology and Engineering, 57(14),* 1463-1473.

[14] **Zainuddin, S., Mahfuz, H., & Jeelani, S.** (2010). Enhancing fatigue performance of sandwich composites with nanophased core. *Journal of Nanomaterials,* 2010, 1-8.

[15] **Saha, M. C., Kabir, M. E., & Jeelani, S**. (2008). Enhancement in thermal and mechanical properties of polyurethane foam infused with nanoparticles. *Materials Science and Engineering: A, 479(1-2),* 213-222.

[16] **Khan, T., Aydın, O. A., Acar, V., Aydın, M. R., Hülagü, B., Bayrakçeken, H., ... & Akbulut, H.** (2020). Experimental investigation of mechanical and modal properties of Al2O3 nanoparticle reinforced polyurethane core sandwich structures. *Materials Today Communications, 24,* 101233.

[17] **Septevani, A. A., Evans, D. A., Annamalai, P. K., & Martin, D. J.** (2017). The use of cellulose nanocrystals to enhance the thermal insulation properties and sustainability of rigid polyurethane foam. *Industrial Crops and Products, 107*, 114-121.

[18] **Şerban, D. A., Weissenborn, O., Geller, S., Marşavina, L., & Gude, M.** (2016). Evaluation of the mechanical and morphological properties of long fibre reinforced polyurethane rigid foams. *Polymer Testing*, *49,* 121-127.

[19] **Yu, Y. H., Choi, I., & Nam, S.** (2014). Cryogenic characteristics of chopped glass fiber reinforced polyurethane foam. *Composite Structures, 107,* 476-481.

[20] **Kim, M. S., Kim, J. D., Kim, J. H., & Lee, J. M.** (2021). Mechanical performance degradation of glass fiber-reinforced polyurethane foam subjected to repetitive low-energy impact. *International Journal of Mechanical Sciences, 194,* 106188.

[21] **Duc, H. M., Huu, D. N., Huu, T. T., Trong, L. L., Nhu, H. L., Ngoc, H. P., ... & Vu, G. N.** (2021). The effect of multiwalled carbon nanotubes on the thermal conductivity and cellular size of polyurethane foam. *Advances in Polymer Technology,* 2021, 1-8.

[22] **Kabir, M. E., Saha, M. C., & Jeelani, S.** (2007). Effect of ultrasound sonication in carbon nanofibers/polyurethane foam composite. *Materials Science and Engineering: A, 459(1-2),* 111-116.

[23] **Xu, X., Liu, F., Jiang, L., Zhu, J. Y., Haagenson, D., & Wiesenborn, D. P.** (2013). Cellulose nanocrystals vs. cellulose nanofibrils: a comparative study on their microstructures and effects as polymer reinforcing agents. *ACS applied materials & interfaces, 5(8),* 2999-3009.

[24] **Yang, G., Kong, H., Chen, Y., Liu, B., Zhu, D., Guo, L., & Wei, G.** (2022). Recent advances in the hybridization of cellulose and carbon nanomaterials: Interactions, structural design, functional tailoring, and applications. *Carbohydrate polymers, 279,* 118947.

[25] **Ibanez Labiano, I., Arslan, D., Ozden Yenigun, E., Asadi, A., Cebeci, H., & Alomainy, A.** (2021). Screen printing carbon nanotubes textiles antennas for smart wearables. *Sensors, 21(14),* 4934.

[26] **Yamane, C., Aoyagi, T., Ago, M., Sato, K., Okajima, K., & Takahashi, T.** (2006). Two different surface properties of regenerated cellulose due to structural anisotropy. *Polymer journal, 38(8),* 819-826.

[27] **Akrami, R., Fotouhi, S., Fotouhi, M., Bodaghi, M., Clamp, J., & Bolouri, A.** (2019). High-performance bio-inspired composite T-joints. *Composites Science and Technology, 184,* 107840.

[28] **Lacki, P., & Derlatka, A.** (2018). Influence of PU foam reinforcement of I-beam on buckling resistance. *Composite Structures, 202,* 201-209.

[29] **Safari, H., Karevan, M., & Nahvi, H.** (2018). Mechanical characterization of natural nano-structured zeolite/polyurethane filled 3D woven glass fiber composite sandwich panels. *Polymer Testing, 67,* 284-294.

[30] **Long, S., Zong, H., Liu, T., & Yao, X.** (2023). Soft impact behavior of composite I-beams. *Composite Structures, 304,* 116477.

[31] **Davids, W. G., Diba, A., Dagher, H. J., Guzzi, D., & Schanck, A. P.** (2022). Development, assessment and implementation of a novel FRP composite girder bridge. *Construction and Building Materials, 340,* 127818.

[32] **Zhou, L., Jiang, L., & Hu, H.** (2016). Auxetic composites made of 3D textile structure and polyurethane foam. *physica status solidi (b), 253(7),* 1331-1341.

[33] **Neje, G., & Behera, B. K.** (2020). Comparative analysis of mechanical behavior of 3D woven spacer sandwich composites with single and double level structures. *Polymer Composites, 41(11),* 4885-4898.

[34] **Luo, H. C., Ren, X., Zhang, Y., Zhang, X. Y., Zhang, X. G., Luo, C., ... & Xie, Y. M.** (2022). Mechanical properties of foam-filled hexagonal and re-entrant honeycombs under uniaxial compression. *Composite Structures, 280,* 114922.

[35] **Yilmaz, B., Akar, E., Kucukkalfa, E., & Yildiz, K.** (2023, June). Direct Foaming Approach for Reinforcing Re-entrant Auxetic Structures for Superior Compressive Properties and Energy Absorption. *In 2023 10th International Conference on Recent Advances in Air and Space Technologies (RAST)* (pp. 01-06). IEEE.

[36] **Kucukkalfa, E., Isikci, G., Yildiz, K., & Cebeci, H.** (2023). Mechanical performance of 3D woven glass fiber I-beam composites with in-situ polyurethane foaming. *Composite Structures, 326,* 117636.

[37] **Assarar, M., Bentahar, M., El Mahi, A., & El Guerjouma, R.** (2015). Monitoring of damage mechanisms in sandwich composite materials using acoustic emission. *International Journal of Damage Mechanics, 24(6),* 787-804.

[38] **Yang, R., He, Y., & Zhang, H.** (2016). Progress and trends in nondestructive testing and evaluation for wind turbine composite blade. *Renewable and Sustainable Energy Reviews, 60,* 1225-1250.

[39] **Masmoudi, S., El Mahi, A., & El Guerjouma, R.** (2014). Mechanical behaviour and health monitoring by acoustic emission of sandwich composite integrated by piezoelectric implant. *Composites Part B: Engineering, 67,* 76-83.

[40] **Tuncel, S.** (2008). TAHRİBATSIZ MUAYENE TEKNOLOJİLERİNDE SON GELİŞMELER: AKUSTİK EMİSYON. *3rd International Non-Destructive Testing Symposium and Exhibition.* Istanbul. Türkiye.

[41] **Huang, J. Q.** (2013). Non-destructive evaluation (NDE) of composites: Acoustic emission (AE). In Non-Destructive Evaluation (NDE) of Polymer Matrix Composites (pp. 12-32). *Woodhead Publishing.*

[42] **Oz, F. E.** (2018). Characterisation of Failure in Composite Materials with Acoustic Emission and Correlation with Micromechanics. *Doctorate thesis, Bogazici University,* Istanbul, Türkiye.

[43] **Chou, H. Y., Mouritz, A. P., Bannister, M. K., & Bunsell, A. R.** (2015). Acoustic emission analysis of composite pressure vessels under constant and cyclic pressure. *Composites Part A: Applied Science and Manufacturing, 70,* 111-120.

[44] **Pascoe, J. A., Zarouchas, D. S., Alderliesten, R. C., & Benedictus, R.** (2018). Using acoustic emission to understand fatigue crack growth within a single load cycle. *Engineering Fracture Mechanics, 194,* 281–300.

[45] **Fotouhi, M., Sadeghi, S., Jalalvand, M., & Ahmadi, M.** (2017). Analysis of the damage mechanisms in mixed-mode delamination of laminated composites using acoustic emission data clustering. *Journal of Thermoplastic Composite Materials, 30(3):*318-340.

[46] **Oskouei, A. R., Ahmadi, M., & Hajikhani, M.** (2009). Wavelet-based acoustic emission characterization of damage mechanism in composite materials under mode I delamination at different interfaces. *Express Polymer Letters, 3(12),* 804-813.

[47] **Malpot, A., Touchard, F., & Bergamo, S.** (2017). An investigation of the influence of moisture on fatigue damage mechanisms in a woven glass-fibre-reinforced PA66 composite using acoustic emission and infrared thermography. *Composites Part B: Engineering, 130,* 11–20.

[48] **Roundi, W., el Mahi, A., el Gharad, A., & Rebiere, J. L.** (2018). Acoustic emission monitoring of damage progression in Glass/Epoxy composites during static and fatigue tensile tests. *Applied Acoustics, 132,* 124–134.

[49] **Lissek, F., Haeger, A., Knoblauch, V., Hloch, S., Pude, F., & Kaufeld, M.** (2018). Acoustic emission for interlaminar toughness testing of CFRP: Evaluation of the crack growth due to burst analysis. *Composites Part B: Engineering, 136,* 55–62.

[50] **Saeedifar, M., Fotouhi, M., Ahmadi Najafabadi, M., & Hosseini Toudeshky, H**. (2015). Prediction of delamination growth in laminated composites using acoustic emission and Cohesive Zone Modeling techniques. *Composite Structures, 124,* 120–127.

[51] **Heidary, H., Ahmadi, M., Rahimi, A., & Minak, G.** (2013). Wavelet-based acoustic emission characterization of residual strength of drilled composite materials. *Journal of Composite Materials, 47(23):*2897-2908.

[52] **Nazmdar, S. M., Yousefi, J., Fotouhi, M., & Ahmadi, N. M.** (2016). Damage evaluation of composite materials using acoustic emission features and Hilbert transform. *Journal of Composite Materials, 50(14):*1897-1907.

[53] **Bohse, J.** (2000). Acoustic emission characteristics of micro-failure processes in polymer blends and composites. *Composites science and technology, 60(8),* 1213-1226.

[54] **Haselbach, W., & Lauke, B.** (2003). Acoustic emission of debonding between fibre and matrix to evaluate local adhesion. *Composites Science and Technology, 63(15),* 2155–2162.

[55] **de Groot, P. J., Wijnen, P. A. M., & Janssen, R. B. F.** (1995). Real-time frequency determination of acoustic emission for different fracture mechanisms in carbon/epoxy composites. *Composites Science and Technology, 55(4),* 405–412.

[56] **Fotouhi, M., Suwarta, P., Jalalvand, M., Czel, G., & Wisnom, M. R.** (2016). Detection of fibre fracture and ply fragmentation in thin-ply UD carbon/glass hybrid laminates using acoustic emission. *Composites Part A: Applied Science and Manufacturing, 86,* 66–76.

[57] **Nikbakht, M., Yousefi, J., Hosseini-Toudeshky, H., & Minak, G.** (2017). Delamination evaluation of composite laminates with different interface fiber orientations using acoustic emission features and micro visualization. *Composites Part B: Engineering, 113,* 185–196.

[58] **Saeedifar, M., & Zarouchas, D.** (2020). Damage characterization of laminated composites using acoustic emission: A review. *Composites Part B: Engineering, 195,* 108039.

[59] **Ali, H. Q., Emami T, I., Khan, R. M. A., Tufani, A., & Yildiz, M.** (2019). Microscopic analysis of failure in woven carbon fabric laminates coupled with digital image correlation and acoustic emission. *Composite Structures, 230,* 111515.

[60] **Marec, A., Thomas, J. H., & el Guerjouma, R.** (2008). Damage characterization of polymer-based composite materials: Multivariable analysis and wavelet transform for clustering acoustic emission data. *Mechanical Systems and Signal Processing, 22(6),* 1441–1464.

[61] **Osa-Uwagboe, N., Udu, A. G., Silberschmidt, V. V., Baxevanakis, K. P., & Demirci, E.** (2023). Damage Assessment of Glass-Fibre-Reinforced Plastic Structures under Quasi-Static Indentation with Acoustic Emission. *Materials, 16(14),* 5036.

[62] **Zhang, K., Tian, W., Chen, P., Ma, C., & Xu, Y.** (2021). Sparsity-guided multi-scale empirical wavelet transform and its application in fault diagnosis of rolling bearings. *Journal of the Brazilian Society of Mechanical Sciences and Engineering, 43,* 1-17.

[63] **Pashmforoush, F., Khamedi, R., Fotouhi, M., Hajikhani, M., & Ahmadi, M.** (2014). Damage Classification of Sandwich Composites Using Acoustic Emission Technique and k-means Genetic Algorithm. *Journal of Nondestructive Evaluation, 33(4),* 481–492.

[64] **Murthy, C. A., & Chowdhury, N.** (1996). In search of optimal clusters using genetic algorithms. *Pattern Recognition Letters, 17(8),* 825-832.

[65] **Bandyopadhyay, S., & Maulik, U**. (2002). An evolutionary technique based on K-means algorithm for optimal clustering in RN. *Information Sciences, 146(1-4),* 221-237.

[66] **Srinivas, M., & Patnaik, L. M.** (1994). Genetic algorithms: A survey. *computer, 27(6),* 17-26.

[67] **Quispitupa, A., Shafiq, B., Just, F., & Serrano, D.** (2004). Acoustic emission based tensile characteristics of sandwich composites. *Composites Part B: Engineering, 35(6–8),* 563–571.

[68] **Ammar, I. B., Karra, C., El Mahi, A., El Guerjouma, R., & Haddar, M.** (2014). Mechanical behavior and acoustic emission technique for detecting damage in sandwich structures. *Applied Acoustics, 86*, 106-117.

[69] **Fotouhi, M., Saeedifar, M., Sadeghi, S., Ahmadi Najafabadi, M., & Minak, G.** (2015). Investigation of the damage mechanisms for mode I delamination growth in foam core sandwich composites using acoustic emission. *Structural Health Monitoring, 14(3),* 265-280.

[70] **Essassi, K., Rebiere, J. L., Mahi, A. E., Amine Ben souf, M., Bouguecha, A., & Haddar, M.** (2022). Health monitoring of sandwich composites with auxetic core subjected to indentation tests using acoustic emission. *Structural Health Monitoring, 21(5),* 2264-2275.

[71] **Harizi, W., Anjoul, J., Santamaría, V. A. A., Aboura, Z., & Briand, V.** (2021). Mechanical behavior of carbon-reinforced thermoplastic sandwich composites with several core types during three-point bending tests. *Composite Structures, 262,* 113590.

[72] **Wu, Y., Pastor, M. L., Perrin, M., Casari, P., & Gong, X.** (2023). Characterisation of damage mechanisms of GFRP-balsa sandwich under 4-point bending based on two-step clustering process in acoustic emission analysis. *Composites Part B: Engineering, 260,* 110774.

[73] **Kucukkalfa, E., Ghaderiaram, A., Yildiz, K., Fotouhi, M., Asadi, A., & Cebeci, H.** (2023). Damage Detection of CNT/CNC-reinforced Foam-cored Sandwich Composites by Acoustic Emission Tests under Flexural Load. *In AIAA SCITECH 2023 Forum* (p. 2030).

[74] **Tabrizi, I. E., Oz, F. E., Zanjani, J. S. M., Mandal, S. K., & Yildiz, M.** (2022). Failure sequence determination in sandwich structures using concurrent acoustic emission monitoring and postmortem thermography. *Mechanics of materials*, *164*, 104113.

[75] **Kucukkalfa E., Dincer M., Karci E., Vural M. A., Yildiz K., Ozden-Yenigun E., Ozkendirci, B., & Cebeci, H.** (2022). Flexural Behaviour Of Polyurethane Foam Filled High Performance 3-D Woven I-Beam Composites. *ECCM 2022 - 20th European Conference on Composite Materials 2020:24–8*.

[76] **Amran, U. A., Salleh, K. M., Zakaria, S., Roslan, R., Chia, C. H., Jaafar, S. N. S., ... & Mostapha, M.** (2021). Production of rigid polyurethane foams using polyol from liquefied oil palm biomass: *Variation of isocyanate indexes. Polymers, 13(18)*, 3072.

[77] **Ji, X. L., Zhou, W., Sun, H., Liu, J., & Ma, L. H.** (2022). Damage evolution behavior of bi-adhesive repaired composites under bending load by acoustic emission and micro-CT. *Composite Structures, 279*, 114742.

[78] **Oz, F. E., Ersoy, N., & Lomov, S. V.** (2017). Do high frequency acoustic emission events always represent fibre failure in CFRP laminates?. *Composites Part A: Applied Science and Manufacturing, 103*, 230-235.

APPENDICES

APPENDIX A: Mechanical Test Results of PU Foams, 3D Woven I-Beam Composites and Sandwich Composites

APPENDIX A: Mechanical Test Results of PU Foams, 3D Woven I-Beam Composites and Sandwich Composites

Table A.1 : Compression test results of each neat and CNT-reinforced PU test specimens.

Specimen	Density (kg/m^3)	Compressive Strength (MPa)	Compressive Modulus (MPa)
N-PU1	109.68	1.01	27.60
N-PU2	111.20	1.05	27.86
N-PU3	112.09	1.06	23.91
N-PU4	109.80	1.01	26.45
N-PU5	113.67	1.13	27.37
N-PU6	113.83	1.11	23.33
Average	111.71±1.66	1.06±0.04	26.08±1.80
0.1CNT-PU1	114.74	1.10	27.00
0.1CNT-PU2	112.85	1.08	32.13
0.1CNT-PU3	111.94	1.08	33.31
0.1CNT-PU4	112.23	1.09	31.10
0.1CNT-PU5	112.21	1.10	28.60
0.1CNT-PU6	113.47	1.16	30.63
Average	112.95±1.05	1.10±0.03	30.63±2.11

Table A.2 : Three-point bending test results of each I-beam composite.

Specimen	Load Bearing Capacity (kN)	Flexural Strength (MPa)	Flexural Modulus (MPa)
H-LBX1	2.83	16.34	481.74
H-LBX2	2.31	13.32	438.34
H-LBX3	1.84	15.79	516.66
H-LBX4	2.06	13.24	466.22
H-LBX5	2.22	14.68	490.17
Average	2.52±0.33	14.67±1.26	478.63±25.95
N-PU-LBX1	3.28	20.70	588.71
N-PU-LBX2	3.96	26.74	707.85
N-PU-LBX3	3.04	20.52	578.30
N-PU-LBX4	3.50	23.87	665.91
N-PU-LBX5	3.52	22.03	608.28
Average	3.46±0.30	22.77±2.32	629.81±49.39
01CNT-PU-LBX1	3.83	23.93	607.14
01CNT-PU-LBX2	4.18	27.90	767.54
01CNT-PU-LBX3	3.17	20.19	606.76
01CNT-PU-LBX4	2.66	19.15	651.22
01CNT-PU-LBX5	3.68	23.43	689.56
01CNT-PU-LBX6	3.70	23.83	699.71
Average	3.54±0.49	23.07±2.84	670.32±56.40

Table A.3 : Compression test results of each neat and CNT-, CNC-, and CNT/CNC-reinforced PU test specimens.

Specimen	Density (kg/m^3)	Compressive Strength (MPa)	Compressive Modulus (MPa)
N-PU1	111.07	0.99	27.19
N-PU2	111.15	0.98	29.75
N-PU3	111.44	0.99	29.98
N-PU4	111.13	0.98	29.94
N-PU5	111.46	0.99	29.94
Average	111.25±0.16	0.99±0.01	29.36±1.09
0.1CNT-PU1	111.38	1.02	34.95
0.1CNT-PU2	109.91	0.97	32.86
0.1CNT-PU3	110.97	1.01	33.54
0.1CNT-PU4	110.47	0.97	33.61
0.1CNT-PU5	109.86	0.99	32.73
0.1CNT-PU6	110.71	0.99	32.93
Average	110.55±0.55	0.99±0.02	33.44±0.75
0.1CNC-PU1	109.09	0.96	31.15
0.1CNC-PU2	109.17	0.95	31.11
0.1CNC-PU3	110.18	0.96	32.07
0.1CNC-PU4	109.23	0.95	30.88
0.1CNC-PU5	109.84	0.96	31.55
Average	109.50±0.43	0.96±0.01	31.35±0.42
0.1CNT/CNC(1:1)-PU1	99.39	0.74	24.10
0.1CNT/CNC(1:1)-PU2	99.76	0.76	25.24
0.1CNT/CNC(1:1)-PU3	99.76	0.76	25.47
0.1CNT/CNC(1:1)-PU4	99.30	0.75	24.68
0.1CNT/CNC(1:1)-PU5	99.34	0.75	24.97
Average	99.51±0.21	0.75±0.01	24.89±0.48
0.1CNT/CNC(1:2)-PU1	103.38	0.83	28.56
0.1CNT/CNC(1:2)-PU2	103.46	0.83	28.69
0.1CNT/CNC(1:2)-PU3	103.33	0.82	28.50
0.1CNT/CNC(1:2)-PU4	103.07	0.80	26.48
0.1CNT/CNC(1:2)-PU5	103.62	0.83	28.32
Average	103.37±0.18	0.82±0.01	28.11±0.82

Table A.4 : Three-point bending test results of each neat and CNT-, CNC-, and CNT/CNC-reinforced PU foam-cored sandwich composites.

Specimen	Load Bearing Capacity (kN)	Flexural Strength (MPa)	Flexural Modulus (MPa)
N-PU1	1.29	14.38	559.37
N-PU2	1.27	14.13	571.87
N-PU3	1.32	13.90	534.31
Average	1.29±0.02	14.14±0.19	555.18±15.62
0.1CNT-PU1	1.36	14.80	588.33
0.1CNT-PU2	1.36	15.08	639.00
0.1CNT-PU3	1.43	15.19	614.55
Average	1.38±0.03	15.02±0.17	613.96±20.69
0.1CNC-PU1	1.31	13.99	609.93
0.1CNC-PU2	1.40	14.94	603.95
0.1CNC-PU3	1.48	16.25	620.37
Average	1.40±0.07	15.06±0.92	611.42±6.78
0.1CNT/CNC(1:1)-PU1	1.23	13.10	500.71
0.1CNT/CNC(1:1)-PU2	1.25	13.25	462.27
0.1CNT/CNC(1:1)-PU3	1.34	13.54	489.75
Average	1.27±0.04	13.29±0.18	484.24±16.17
0.1CNT/CNC(1:2)-PU1	1.27	13.42	521.42
0.1CNT/CNC(1:2)-PU2	1.21	13.00	479.50
0.1CNT/CNC(1:2)-PU3	1.32	14.44	529.17
Average	1.27±0.04	13.62±0.60	510.03±21.82

CURRICULUM VITAE

Name Surname : Eyüphan KÜÇÜKKALFA

EDUCATION :

- **B.Sc.** : 2021, Istanbul Technical University, The Faculty of Aeronautics and Astronautics
- **M.Sc.** : 2024, Istanbul Technical University, The Faculty of Aeronautics and Astronautics

PROFESSIONAL EXPERIENCE AND REWARDS:

- 2022-2024 Research Assistant at Istanbul Technical University at Aviation Institute.

PUBLICATIONS, PRESENTATIONS AND PATENTS ON THE THESIS:

- **Kucukkalfa E.,** Dincer M., Karci E., Vural M. A., Yildiz K., Ozden-Yenigun E., Ozkendirci, B., & Cebeci, H. 2022: Flexural Behaviour Of Polyurethane Foam Filled High Performance 3-D Woven I-Beam Composites, ECCM 2022 - 20th European Conference on Composite Materials, 26-30 June 2020, Luzern, Switzerland.
- **Kucukkalfa, E.,** Ghaderiaram, A., Yildiz, K., Fotouhi, M., Asadi, A., & Cebeci, H. 2023: Damage Detection of CNT/CNC-reinforced Foam-cored Sandwich Composites by Acoustic Emission Tests under Flexural Load, AIAA Scitech 2023 Forum, 23-27 January 2023, National Harbor, MD, United States.

OTHER PUBLICATIONS, PRESENTATIONS AND PATENTS:

- **Kucukkalfa, E,** Isikci, G., Yildiz, K, Cebeci, H. 2023. Mechanical Performance of 3D Woven Glass Fiber I-beam Composites with In-situ Polyurethane Foaming, *Composite Structures*, 326, 117636.
- **Kucukkalfa, E.,** Ok, O., & Yildiz, K. 2024: Energy Absorption Characteristics of Elastomeric Nanoparticle Reinforced Polymeric Foam-Filled Auxetic Structures Under Cyclic Compression, AIAA Scitech 2024 Forum. 8-12 January, Orlando, Florida, USA.
- Ok, O., **Kucukkalfa, E.,** Yildiz, K. & Cebeci, H. 2024: Viscoelastic Properties of Carbon Nanotube Reinforced Polyurethane Foams through Dynamic Mechanical Analysis, AIAA Scitech 2024 Forum. 8-12 January, Orlando, Florida, USA.

- Calaner, N., Kivandik, E.B., **Kucukkalfa, E.,** & Yildiz, K. 2024: Progressive Reinforcing of Re-entrant Auxetic Structures by Direct Polyurethane Foaming within Unit Cells, AIAA Scitech 2024 Forum. 8-12 January, Orlando, Florida, USA.
- Arslan, D., Dincer, M., Akyazici, Z. N., **Kucukkalfa, E.,** Demirer, E. R., Yildiz, K., Ozkendirci, B., Ozden-Yenigun, E. & Cebeci, H. 2023: In-situ Cure Monitoring of 3D Woven Composites with a Multifunctional CNT Sensor. 23rd International Conference on Composite Materials (ICCM23), Belfast, Northern Ireland.
- Yilmaz, B., Akar, E., **Kucukkalfa, E.,** & Yildiz, K. 2023: Direct Foaming Approach for Reinforcing Re-entrant Auxetic Structures for Superior Compressive Properties and Energy Absorption. 10th International Conference on Recent Advances in Air and Space Technologies, Istanbul, Türkiye.